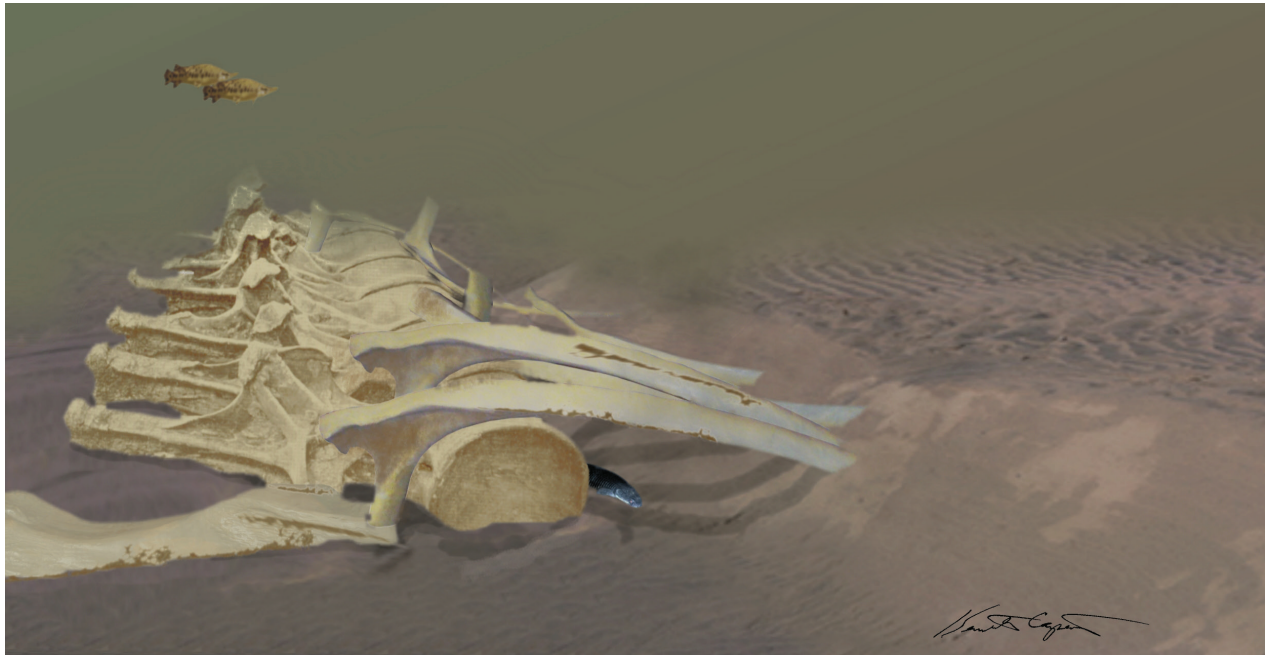# HYDRAULIC MODELING AND COMPUTATIONAL FLUID DYNAMICS OF BONE BURIAL IN A SANDY RIVER CHANNEL

Kenneth Carpenter

Theme Issue
An Ecosystem We Thought We Knew—
The Emerging Complexities of the Morrison Formation
SOCIETY OF VERTEBRATE PALEONTOLOGY
Annual Meeting, October 26 – 29, 2016
Grand America Hotel
Salt Lake City, Utah, USA

Editors

Douglas A. Sprinkel
Azteca Geosolutions
801.391.1977
GIW@utahgeology.org
dsprinkel@gmail.com

Bart J. Kowallis
Brigham Young University
801.422.2467
bkowallis@gmail.com

Steven Schamel
GeoX Consulting, Inc.
801-583-1146
geox-slc@comcast.net

Thomas C. Chidsey, Jr.
Utah Geological Survey
801.537.3364
tomchidsey@utah.gov

John R. Foster
Utah Field House of
Natural History State Park
Museum
435.789.3799
johnfoster@utah.gov

Society of Vertebrate Paleontology Editors

Kelli C. Trujillo — University of Wyoming
Cary Woodruff — University of Toronto
Octavio Mateus — Universidade Nova de Lisboa

Production

Cover Design and Desktop Publishing
Douglas A. Sprinkel

Cover

*A partial **Camarasaurus** skeleton about to be buried by an advancing subaquatic dune.*

UGA Board

2020 President	Leslie Heppler	lheppler@utah.gov	801.538.5257
2020 President-Elect	Riley Brinkerhoff	riley.brinkerhoff@gmail.com	406.839.1375
2020 Program Chair	Paul Inkenbrandt	paulinkenbrandt@utah.gov	801.537.3361
2020 Treasurer	Greg Gavin	greg@loughlinwater.com	801.538.4779
2020 Secretary	Elliot Jagniecki	ejagniecki@utah.gov	801.537.3370
2020 Past President	Peter Nielsen	peternielsen@utah.gov	801.537.3359

UGA Committees

Education/Scholarship	Zack Anderson	zanderson@utah.gov	801.538.4779
Environmental Affairs	Craig Eaton	eaton@ihi-env.com	801.633.9396
Geologic Road Sign	Greg Gavin	greg@loughlinwater.com	801.541.6258
Historian	Paul Anderson	paul@pbageo.com	801.364.6613
Membership	Rick Ford	rford@weber.edu	801.626.6942
Outreach	Greg Nielsen	gnielsen@weber.edu	801.626.6394
Public Education	Paul Jewell	pwjewell@mines.utah.edu	801.581.6636
	Matt Affolter	gfl247@yahoo.com	
Publications	Paul Inkenbrandt	paulinkenbrandt@utah.gov	801.537.3361
Publicity	Paul Inkenbrandt	paulinkenbrandt@utah.gov	801.537.3361
Social/Recreation	Roger Bon	rogerbon@xmission.com	801.942.0533

AAPG House of Delegates

2017–2020 Term	Tom Chidsey	tomchidsey@utah.gov	801.537.3364

State Mapping Advisory Committee

UGA Representative	Bill Loughlin	bill@loughlinwater.com	435.649.4005

Earthquake Safety Committee

Chair	Grant Willis	gwillis@utah.gov	801.537.3355

UGA Website — www.utahgeology.org

Webmaster	Paul Inkenbrandt	paulinkenbrandt@utah.gov	801.537.3361

UGA Newsletter

Newsletter Editor	Bill Lund	uga.newsletter@gmail.com	435.590.1338

Become a member of the UGA to help support the work of the Association and receive notices for monthly meetings, annual field conferences, and new publications. Annual membership is $20 and annual student membership is only $5. Visit the UGA website at www.utahgeology.org for information and membership application.

The UGA board is elected annually by a voting process through UGA members. However, the UGA is a volunteer-driven organization, and we welcome your voluntary service. If you would like to participate please contact the current president or committee member corresponding with the area in which you would like to volunteer.

Hydraulic Modeling and Computational Fluid Dynamics of Bone Burial in a Sandy River Channel

Kenneth Carpenter

Museum of Natural History, University of Colorado, Boulder, CO 80302 USA; Kenneth.Carpenter-1@colorado.edu

ABSTRACT

An oval recycling flume with live-beds (moveable) of medium and very coarse grained sands were used to explore the process of bone burial as a precursor to fossilization. Two-dimensional computation fluid dynamics was used to visualize and interpret the flow turbulence around bones. Results show that a water mass approaching and passing a static bone (obstruction) is subjected to flow modification by flow separation, flow constriction, and flow acceleration producing complex flow patterns (turbulence). These complex patterns include an upstream high-pressure zone, down flows, and vortices (with flow reversal near the bed) causing bed shear stress that produce bed erosion. Downstream of the bone, the water mass undergoes flow deceleration, water recirculation (turbulence eddies), flow reattachment, low-pressure zone (drag), and sediment deposition. Scour plays a crucial role by undercutting bone on the upstream side and may cause the bone to settle into the bed by rotation or sliding. Scour geometry is determined by bone size and shape, approaching flow velocity and angle to flow, flow depth, bed topography, and bed friction. Drag on the downstream side of the bone causes scoured sediment deposition, but burial by migrating bed forms is the most important method of large bone burial. Bone may be repeatedly buried and exposed with renewed scour. However, each episode of scour may lower the bone deeper into the bed so that it essentially buries itself. No difference in these effects were noted between experiments using fine or coarse grain sizes. This experimental work is then used to interpret the possible history of bone burial in the Upper Jurassic Morrison Formation on the bone wall inside the Quarry Exhibit Hall at Dinosaur National Monument, Utah.

INTRODUCTION

The interaction of bone and moving water has been explored using laboratory flumes to investigate taphonomic bias caused by bone dispersal from sliding, rolling, and floating in moving water, and also abrasion to bone by impact with sand in suspension or on the bed (Voorhies, 1969; Dodson, 1973, Boaz and Behrensmeyer, 1976; Hanson, 1980; Boaz, 1982; Frison and Todd, 1986; Coard and Dennell, 1995; Blob, 1997; Morris, 1997; Trapani, 1998; Coard, 1999; Fernandez-Jalvo and Andrews, 2003, 2016; Pante and Blumenschine, 2010; Kaufmann and others, 2011; Thompson and others, 2011; Griffith and others, 2016). The flumes used in these studies are a form of physical hydraulic modeling, which may be predictive to obtain a specific answer to a specific problem or may be investigative to further the understanding of hydrological processes (Grayson and others, 1992; Blöschl and Sivapalan, 1995). For example, flumes have been used to analyze design and operation issues in hydrauling engineering, including bed-load sediment transportation, debris transport, flow and lo-

cal scour around hydraulic structures, or obstructions (e.g., bridge abutments, dikes, low walls, coastal piers), and flow around deflectors in stream rehabilitation (summarized in Hoffmans and Verheij, 1997; Ettema and others, 2000). These process models are often used in conjunction with numerical modeling (e.g., computational fluid dynamics) to understand what is observed in the physical models. Additionally, numerical modeling is used as a predictive tool for fluvial systems when certain parameters change (e.g., 100- to 500-year flood, Horritt and Bates, 2002). Predictive numerical modeling has greatly improved with the integration of remote sensing data of the real world (e.g., Matgen and others, 2007; Schumann and others, 2009).

The reliability of flume modeling is dependent on geometric similitudes, which are important prerequisites for dynamic similitudes (Franco, 1978; Ettema and others, 2000). Similitude refers to how close the flume conditions simulates or matches real-world conditions. Perfect similitude is not practical and not necessary given that specific problems are typically being investigated. By limiting similitude to specific conditions, complex real-world situations become manageable through restricting variables and allowing for experiment repeatability. For example, studies of bed erosion (local scour) around bridge abutments do not simulate specific river types (braided, meandering, or anastomosing) because the investigation is only concerned with the interaction of flowing water, the bed material, and the obstacle (i.e., the abutment) (Ettema and others, 2000). Likewise, differential bone transport studies have not included river type because the problem investigated is the interaction of flowing water and bone. Such limited modeling gives generalized results that can then help to understand or interpret real world events, past or present (e.g., Voorhies, 1969; Boaz, 1982; Morris, 1997; Carpenter, 2013, 2016). Many of these flume bone transport studies are similitudes of sheet-wash conditions because water depths are only a few centimeters and the bones are not always completely submerged; deeper water modeling is rarely done. Water depth is a known major factor in hydraulic modeling as discussed below in the section on the basics of flow dynamics.

The error between the real-world example (called the "prototype" in hydraulic modeling) and the simili-

tudes increases with scaling due to the unscalable properties of water, such as flow inertia, viscosity, and surface tension. Other properties are also fixed, such as gravity and the lower limit of grain size. Down scaling of grain size to silt and clay size is difficult because of how differently these smaller particles behave in water (e.g., settling velocities). This scaling problem of grain size complicates the scaling of bed forms. Despite these limitations, a broad range of flow and dynamic situations can be analyzed with flumes either by minimizing down scaling, down scaling some but not all components, using particles other than sand, or using fluids other than water (Franco, 1978; Ettema and others, 2000; Ettema and Muste, 2004).

The bone transport experiments are a form of actualistic taphonomic investigation. What has not been studied in detail is what happens after bone transportation stops. How do bones become buried in order to become fossilized? Uncontrolled "wild" field studies are of limited value because the burial of bones are rare, unpredictable events, and when they do occur, visibility of the processes is negligible because of water depth, suspended sediment, and water turbulence. At best, studies of such examples are post-process interpretation (figure 1; e.g., Boaz, 1982). Very little controlled experimental work has examined the burial process in a fluvial environment. One exception was the preliminary work presented previously as part of a larger work on the bone accumulation in the Upper Jurassic Morrison Formation at the Carnegie Quarry in Dinosaur National Monument (Carpenter, 2013). That study used casts of bones in a creek to better understand the effects of bone obstruction (not transport) to water flow and how that may influence burial. This present study delves further into the processes of bone burial in a fluvial environment by using flume experiments and computational fluid dynamics to interpret the flow dynamics (Carpenter, 2016). In some ways this study was preceded by Johnson (1957) who used a flume to study the scour burial of shells.

The advantages of flume experimentation are multiple: (1) to make real world problems manageable, (2) to control variables for a particular issue, and (3) replicability (Ettema and others, 2000). In the example of the cow carcass (figure 1), the events leading up to the car-
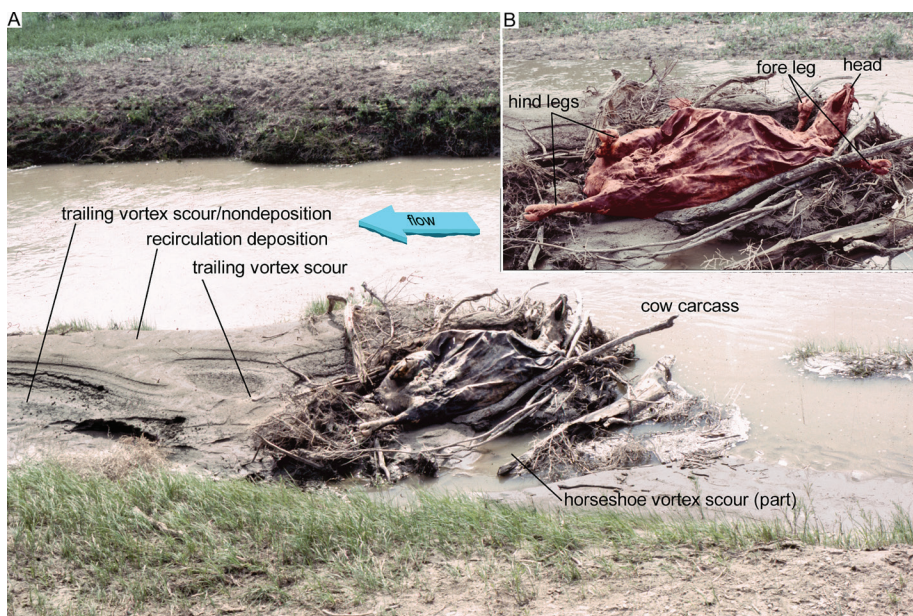
Figure 1. Limitations of non-flume studies to interpret prefossilization burial. (A) Cow carcass in a river channel as an example of real-world observation to understand bone burial is limited and mostly a post-process interpretation. Inset (B) shows the carcass highlighted as a guide to (A).

cass being deposited where it was found are unknown. This includes the origin, timing, and actions leading to carcass entrainment in the water, how far transport occurred, and the effects on fluvial flow patterns once the carcass became stationary; these effects can only be inferred, not observed (figure 1A). It is also not known if the carcass remained at this spot and decayed in place. More importantly for this study is if *in situ* burial eventually took place and if so, how?

A major question of the flume experiments is: can the generalized results be used to interpret a fossil bone site in a manner analogous to how flume bone dispersal studies are used to understand taphonomic bias and bone orientation? The bone wall inside the Quarry Exhibit Hall at Dinosaur National Monument is used as a case study.

MATERIALS AND METHODS

To study bone burial, a prerequisite for fossilization, a variety of casts and real bones were used (table 1) in an elliptical ("racetrack") flume with a moveable bed of sand. The fiberglass covered plywood and stud-framed flume has an axial length of 362 cm and a width of 213 cm. The functional part of the flume, the trough, has a width of 75 cm, a floor of 49,314 cm², and walls 50 cm tall. The interior of the trough was coated with multiple layers of fiberglass cloth and polyester resin. Water dimensions for various depths used in the experiment are given in table 2 (water slope = 0). A paddle

Table 1. Bones used in the flume experiments. Abbreviations: r = real bone; c = cast bone.

Alligator mississippiensis skull (r)
Allosaurus fragilis skull (c)
Bos taurus skeletal elements (r)
Camarasaurus lentus vertebra (c)
Canis familiaris skull (r)
Castor canadensis skull (r)
Dryosaurus skull (c)
Felis domesticus skull (r)
Odocoileus hemionus skeletal elements (r)
Varanus salvator vertebral column (r)

Table 2. Physical parameters of the water in the flume.

Depth (cm)	Hydraulic area (cm²)	Hydraulic radius (cm)	Volume (cm³)
30	2250	16.6	1,479,420
35	2625	18.1	1,725,990
40	3000	19.4	1,972,560

wheel rather than pump was used to move the water unidirectionally so as to pulse the water. Pulsing caused minor fluctuations in velocity and water depth mimicking the unsteady, nonuniform flow of rivers. The paddle wheel had a radius of 42.7 cm and a circumference of 268.25 cm;

each of the eight paddles had an area of 800 cm^2. The paddle wheel was belt driven using a 230-volt, three-phase motor, with an auxiliary external fan to prevent overheating. Speed was controlled with a Teco inverter motor speed regulator and water velocities recorded with a Vernier flow rate sensor connected to a Lenovo Yoga 700 convertible laptop. As with many flume studies, water temperature was not considered significant and not recorded.

Two types of commercial sand were used to determine if grain size had any effect on bone burial. One was a fine white quartz sand with a D_{60} of 0.35 mm, and another of poorly sorted, coarse quartz-feldspar playsand with a D_{60} of 0.9 mm (range 0.6–1.0 mm). The sands were dry screened to remove the smaller fractions (<0.35 mm and <0.6 mm, respectively), then washed to remove any dust, which would cloud the water reducing visibility. An exterior swimming pool filter pump was used to filter any remaining particles from the flume water. An acrylic deflector at one end of the race track diverted the water and sand towards the middle of the study section of the trough; otherwise flow would be confined centripetally against the outer side. Bones were placed on a smooth bed that was at least 2 cm deep at the start of each run and in long duration runs, bed structures were allowed to develop naturally (figure 2). The effects of various flow speeds (0.25 to 2 m/s) on bone burial were investigated, but most with a mean horizontal velocity (U) between 0.5 and 1 m/s, which lies within the dune stability field (figure 3). Lower velocities were used in clear water scour studies (scour developed but no bed forms developed upstream), which were of short duration (minutes) and repeated to understand various events, such as the initiation of local scour (i.e., scour at the bones). Higher velocities were used in live bed studies in which bed forms developed and passed over the bones. An acrylic window in the side of the flume provided an underwater view of the objects resting on the bed. Photographs were taken through the window, as well as underwater with a Nikon Coolpix waterproof digital camera. Flow was occasionally stopped to allow plan-view photography without turbulence distortion of water surface.

Flowsquare 4.0 (Minamoto, 2013) computational fluid dynamics (CFD) software on a Lenovo ThinkCen-
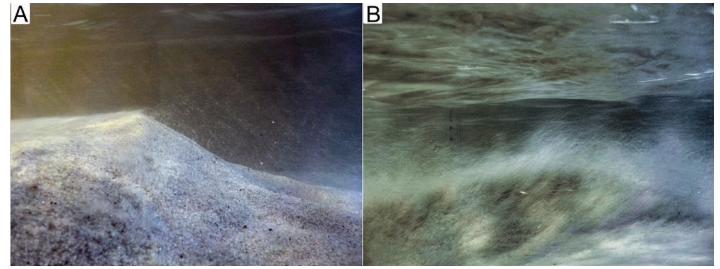

Figure 2. Sedimentary structures in the flume. (A) 20-cm-tall dune with crest-shedding fine grains into the water column, water velocity about 1 m/s. (B) Turbulent flow around a dune, water velocity about 2 m/s. Because of the extreme turbulence, few experiments were conducted at this velocity; most were between 0.5 and 1 m/s.
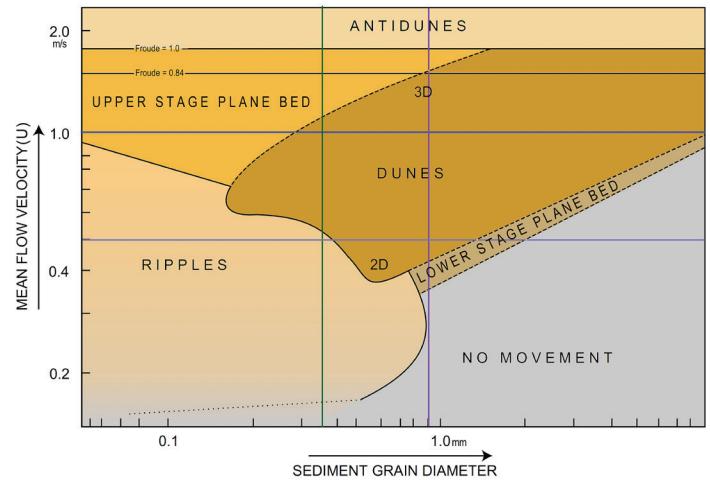

Figure 3. Stability field for various bed form states relative to grain size and flow velocity. Vertical axis are grain sizes (median D_{60}) used in this study (green = 0.35 mm; purple = 0.9 mm). Horizontal axes bracket the average velocities for most studies (light blue = 0.5 m/s; blue = 1 m/s). Note that the intercept of the grain size axes and velocity axes lie with the dune stability field. The critical velocity for grain movement is variable and is denoted by the dotted line. Modified from Southard and Boguchwal (1990).

tre desktop computer was used to understand the complex flow field developed when a bone obstruction is encountered. Flowsquare can simulate incompressible non-reacting flows, such as flowing water in a two-dimensional channel. To simplify analyses of flow obstruction in an open channel, the approaching flow was set as laminar, with steady uniform mean velocity (U; these are given below with the experiments), uniform

flow depth (also given below with examples), and an immobile lower (bed) wall boundary layer. Data input is in the form of a Bitmap of the obstacle and boundaries, and a control text file containing modeling parameters (fluid density, fluid velocity, etc.; grid size, duration of the run, etc.). The number of grid points were usually set as X = 574, Y = 187, occasionally higher for greater detail. Visualization as a gradient of colors (blue = lowest values, yellow = intermediate values, red = highest values; peak values are given in the captions) and flow vectors are displayed in real time and the results saved at specified intervals as Bitmap files for post-analysis and for use in figures. When the program is executed, the continuity equation and the equation for momentum is solved for each grid cell (mesh) as the "flow" moves with each time step from the inflow boundary (left margin of the grid) towards the outflow boundary (right margin).

To maximize similitude in the flume, real bone and casts of full-size dinosaur bones were used. Because the intent of the flume studies was not bone transportation, which has been investigated by others listed above, weights were tied or inserted within skulls to keep the plastic resin casts on the sediment surface so that they acted as stable obstacles to flow. Skulls were used to determine how an open structure affected events leading to burial, and incidentally provided information about the burial of the isolated skulls.

Terminology used below is given in figure 4. Except where noted, flow is left to right in all figures.

BASICS OF FLOW DYNAMICS AROUND AN OBSTRUCTION

The hydraulic literature is rich with studies about the impact a hydraulic structure (a.k.a., obstruction) resting on the bed has on unidirectional flow (e.g., Lefeuvre, 1965; Dargahi, 1990; Olsen and Melaaen, 1993; Brørs, 1999; Ettema and others, 2000; Istiarto, 2001; Biron and others, 2005; Smith and Foster, 2005; Tritico and Hotchkiss, 2005; Cataño-Lopera and García, 2006; Carré and others, 2007; Bocchiola, and others, 2008; Dey and others, 2008; Kirkil and Constantinescu, 2010; Bocchiola, 2011; Mazumder and others, 2011; Euler and Herget, 2011, 2012; Termini, 2011; Dixen and oth-
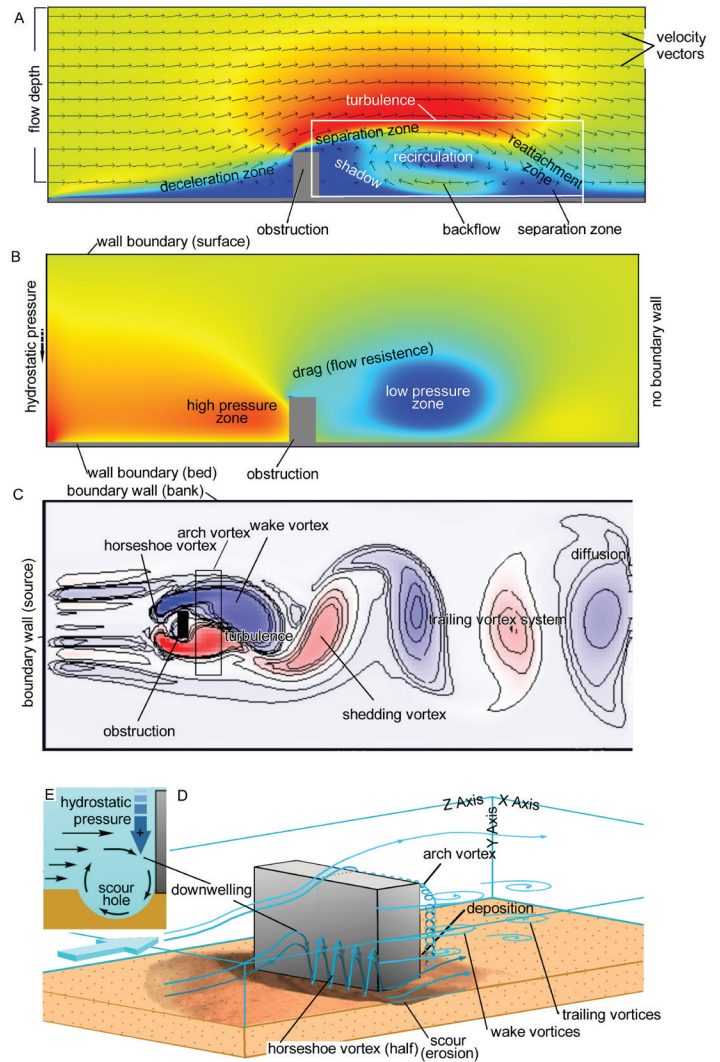

Figure 4. Illustration of terminology used. (A) Water velocity; color gradient from slowest (blue), intermediate (yellow), and fastest (red). (B) Water pressure; color gradient from lowest (blue), intermediate (yellow), and highest (red). (C) Water vortices in plan view (red and blue denote different vortices; intensity of color indicates relative speed of vortices). (D) Water vortices in three-dimensional (3-D) view. (E) Scour detail in cross section (length of arrows corresponds to relative velocities).

ers, 2013; Menzel and others, 2013; Maity and Mazumder, 2014), and most importantly for this study—the resulting burial of low obstructions (e.g., Dill, 1958; Inman and Jenkins, 1996, 2005; Jenkins and others, 2007; Cataño-Lopera, and others, 2011; Friedrichs and others, 2016). These studies corroborate one another about

underlying principles of the flow regime around an obstacle, as well as the important effects of obstacle shape, water depth, and water velocity.

An obstacle causes flow resistance, creating complex three-dimensional (3-D) flow separation, or turbulence. These flow separations produce areas of acceleration and deceleration (figure 4A, vector arrows). Because water is a non-compressible fluid, differential pressure gradients, which is drag, develop around the obstacle (figure 4B). The pressure gradients form because the same mass of water on the upstream side of the obstacle is squeezing past the obstacle (figures 4C and 4D), the so-called "thumb on the garden hose" effect.

Near and at the bed, changes in flow dynamics produce turbulence and bed shear stress along the X-, Y- and Z-axes (figure 4E). The highest values of near-bed turbulence occur in front of and immediately adjacent to the obstacle thereby causing scour, i.e., bed erosion (figure 4D). This turbulence is manifested as a horizontal helical or horseshoe vortex (figures 4C and 4E), which forms as approaching water is forced down due to overlying hydrostatic pressure and continued inflow of water from upstream (figure 4D). If the water is shallow, velocity high, and hydrostatic pressure low, part of the water deflects upwards producing a dome or crest of water above the obstacle as a standing wave. The downward flow is deflected upstream by the bed because of the presence of a low-pressure gradient due to drag of the bed effect (note the narrow lower pressure zone above the bed in figure 4B and narrow deceleration zone delineated by arrow length in figures 4A and 4D). The upstream recirculation flow then reincorporates into the downstream flow producing a localized spiral motion of the water (figure 4D). However, the constant inflow of water coming from upstream produces a high-pressure zone and the water spirals laterally in both directions as a helix towards the regions of lower pressure. Once past the obstacle, water coming from upstream deflects the helix in the downstream direction so that the helix has a horseshoe shape, hence is known as a horseshoe vortex (figure 4C). The energy of helical motion erodes the bed producing a horseshoe-shaped scour when the ratio between the approaching water velocity and critical velocity (minimum water velocity to initiate grain movement) is about 0.45 m/s (Dou and

Jones, 2000). As the helix extends downstream past the obstacle, the energy dissipates and sediment that was transported from the scour settles out when the velocity falls below transport threshold.

For obstructions that do not extend above the water surface, flow above the hydraulic pressure threshold for down welling deflects up and over or around (figure 4A and 4D). Flow separation results in an arch-shaped vortex on the downstream side of the obstruction, as well as shedding wake vortices. This trailing system of wake vortices diffuses as the energy dissipates (figure 4C). Backflow in the recirculation zone deposits sediment eroded by the horseshoe vortex (compare figure 4C with 4A). This region is also marked by a low-pressure zone (figure 4B). The low pressure zone also plays a role in generating lift; this was discussed elsewhere (Carpenter, 2013).

TESTING SIMILITUDE OF BONE IN FLOWING WATER

The most basic question is whether bone as an obstacle affects water flow in the same manner as other obstacles used in hydraulic studies. To test this, a cow femur was immersed in shallow water (10 cm) and subjected to unidirectional flowing water (U = 0.25 m/s) (figure 5). The femur was initially supported on the bed by the distal condyles, which sank into the substrate a few millimeters until it reached the competency of the sand. Shortly after flow initiated, clear water scour developed on the upstream side as a horizontal helical flow at the base of the femur and progressed rapidly until the femoral shaft rested on the bed (figures 5A to 5C). Thus, support shifted from the distal condyles to the shaft. Sediment scoured on the upstream side (figures 5D and 5E) produced the characteristic horseshoe-shaped scour (figure 5F), with the eroded sediment deposited downstream adjacent to the femoral shaft (figure 5D). Analysis of the distal end of the femur with CFD (figure 5G) showed that there was an increase in pressure as the water piled up in front of the condyles. The region of maximum pressure is also where the horseshoe scour developed (compare figure 5G with figure 5F). The results of this first study revealed the similitude of bone as an obstacle to uniform flow hydraulics.
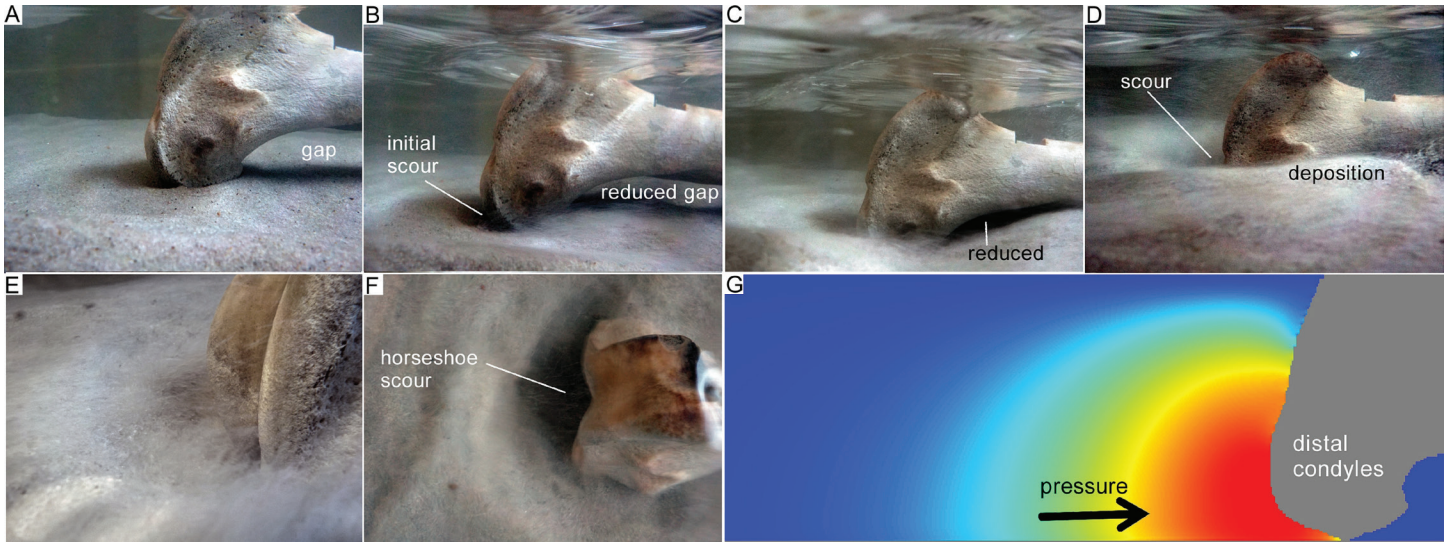
Figure 5. Distal end of a cow femur as an obstruction. Conditions: sand $D_{60} = 0.35$ mm, water depth = 30 cm, U = 0.25 m/s. (A) At start, the femur is supported by the distal condyles leaving a gap below the shaft. (B) Initial scour begins at the condyles causing them to sink into the bed and reducing the gap below the shaft. (C) Continued scour eventually eliminates the gap and the shaft rests on the bed. (D) Sediment removed by the scour is deposited posterolaterally adjacent to the condyles. (E) Close-up view along the axis of the helical vortex; sand is spirally towards viewer. (F) Horseshoe scour seen in plan view. (G) CFD analysis showing water pressure gradient. The region of maximum pressure (red, peak at 1125 Pascals [Pa]) explains why the horseshoe scour develops immediately in front of the femur.

FLUME EXPERIMENT RESULTS

The process leading to burial for all bones can be divided into two phases: clear water phase, in which most bed events occur in the vicinity of the bone and no bed forms develop upstream, and live bed phase which involves migrating bed forms. Each of these in turn can be further divided into events and are listed numerically to keep each distinct. The behavior of the bones as obstacles in unidirectional flow were similar reflecting basic underlying principles and therefore are treated together to minimize repetitiveness; skulls, however, are treated separately from postcrania.

Clear Water Phase

Skulls

The skulls used include casts of *Allosaurus* (figures 6 and 7) and *Dryosaurus* (figure 8) and real skulls of *Alligator* (figure 9), *Canis* (figure 10), and *Castor* (figure 11). No large skulls (e.g., *Bos*) were included owing to limitations imposed by flume width.

1. For skulls aligned perpendicular to flow, the skulls initially pivoted horizontally on the bed from the increased water pressure until reaching equilibrium with bed friction (compare figures 6A and 6B to figures 8A and 8C). The exceptions were the beaver skull (discussed further below) and the *Alligator* skull, palate side down, in which the teeth acted as anchors in the bed.

2. Immediately upon initiation of clear water phase, bed erosion is evidenced by a depression, the scour hole, forming directly on the upstream side of the skull (frontal scour) and by sand grains entrained into the helical vortex (e.g., figures 6B and 8C). This scour forms in the high-pressure zone at the skull-bed interface, which does not necessarily correspond to highest velocities (compare figure 6M with 6N; figure 9J with 9K; figure 10G with 10H).

3. This initial scour began as a short segment on the bed near mid-skull as the pressure gradient grew very rapidly (figure 6N) and the velocity of the helical vortex exceeded the critical velocity threshold of the sand grains (see figure 3, black lines and dashes).
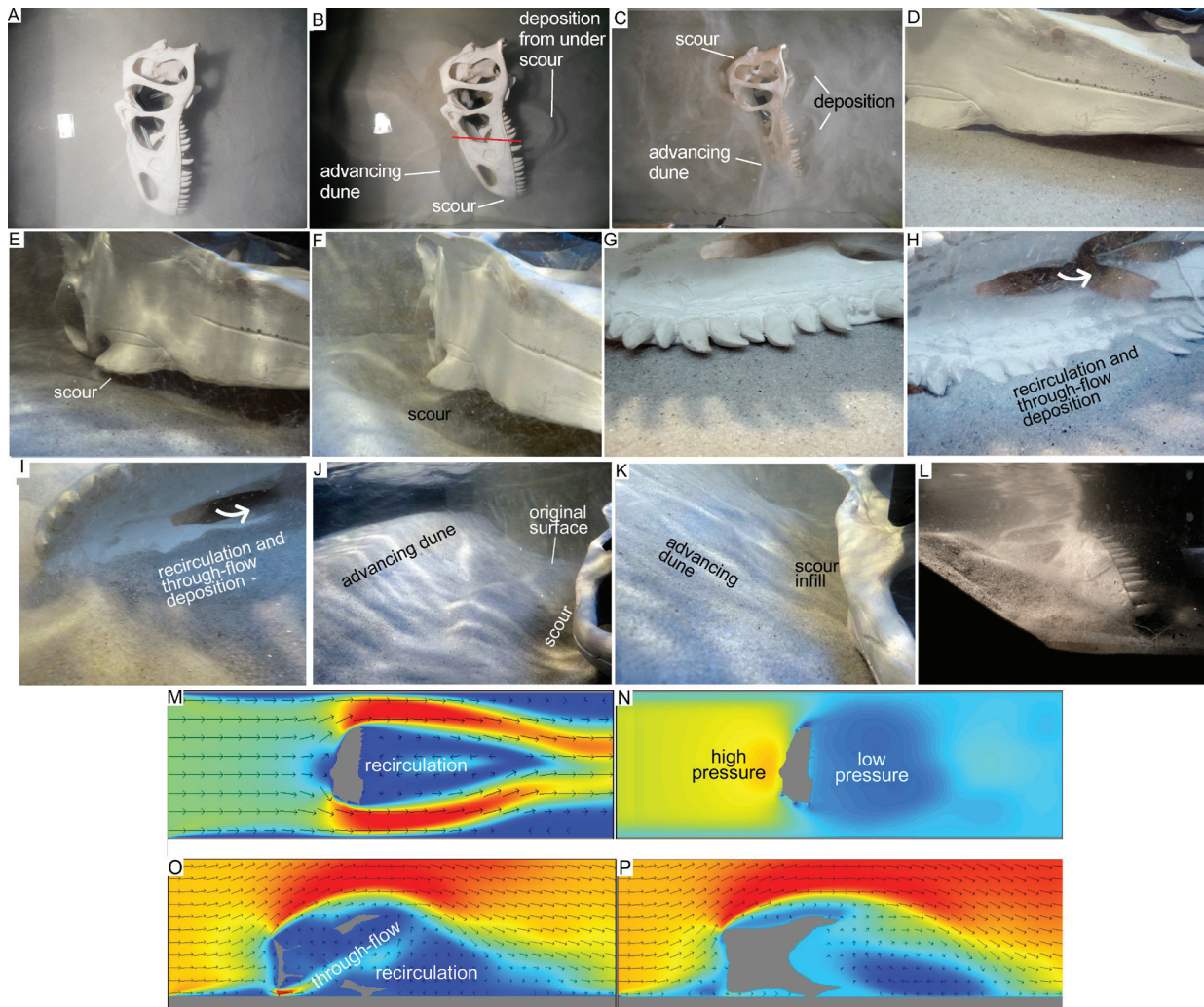
Figure 6. The effects of flow on an *Allosaurus* skull cast resting on a live-bed of medium sand. Conditions: sand D_{60} = 0.35 mm, water depth = 30 cm, U = 0.5 m/s. (A) Skull placement at start. (B) Pivot of skull (about 35°) before scouring began. Scour and deposition co-occur. Red line is approximate location of figures 6M and 6N. (C) Burial of skull by advancing dunes. Detail upstream side of skull. (D) Start position of skull. (E) Initial scour and undercutting of skull on upstream side. White specks and streaks are sand particles in suspension. (F) Extended under-scouring, just before skull slumped into scour hole. Detail downstream side of skull. (G) Start position of skull. (H) Initial deposition from through-flow (arrow) and recirculation. (I) More advanced stage of deposition from through-flow (arrow) and recirculation. Burial by dune. (J) Advancing dune. Scour still occurring. (K) Infill of scour by cascading sand on lee side of dune. (L) Burial of skull by dune. (M) CFD of horizontal velocity (U = 0.5 m/s) around the skull in map view. Note a near doubling of the flow velocity, from 0.5 m/s to 1 m/s as it passes around the ends of the skull. (N) CFD pressure fields peak at 4922 Pa on the upstream side of the skull and drop to 210 Pa on the downstream side. (O) CFD showing complex flow dynamics through open skull (cross section through antorbital fenestrae approximately at red line in 6B); peak U = 1.9251 m/s. (P) Vectors showing simple flow dynamics over flesh covered skull (without lower jaws); peak U = 1.9251 m/s.

4. The helical vortex rapidly grew in width (Z axis) until the lateral by-pass flow (X axis) forced the vortex to curve downstream producing the horse-shoe-shaped vortex (figure 6M), which was man-ifested on the bed by development of the charac-teristic horseshoe scour (figures 6B and 8C).

5. Eroded sediment moved to the lee side of the skull by the wake vortex system where it is de-

Figure 7. The effects of flow on an *Allosaurus* skull cast resting on a live-bed of coarse sand. Conditions: sand D_{60} = 0.9 mm, water depth = 20 cm, U = 1 m/s. Overall behavior of the sand is similar to finer grained sand. (A) Scour on upstream side. (B) Burial by advancing dune (streaks in lower right are sand grains in brief suspension). (C) View downstream showing stoss side of advancing dune, skull palate side this time facing upstream; flow stopped for photography. (D) Burial of skull by advancing dune; flow stopped for photography. (E) Profile of advancing dune, skull on right; flow stopped for photography.

posited by subcritical recirculation flow, which is a low-pressure zone (figures 6M to 6O). Other sediment is carried through the skull and deposited in the low-pressure zone on the downstream side (figures 6B, 6H, 6I, 6O, and 8C).

6. Propagation of the frontal scour depth (Y axis) and length (X axis, mostly in the downstream direction), ultimately undercut the skull (figures 6E, 6F, and 8D). The dual frontal scour zones reported by Euler and Herget (2012) were not seen, but may be due to the higher flow velocity.

7. When the frontal scour undercut beyond the center of gravity, the mass of the unsupported portion of the skull underwent rotational motion in an upstream direction (X axis) causing it to tilt into the scour (Y axis). Renewed undercutting by the horseshoe vortex caused the upstream side of the skull to settle deeper into the substrate (compare slope of quadrates in figures 8B and 8D). This is the same principle that makes stone imbrication in river channels, even of several hundred-kilogram boulders (see Euler and others, 2017, figure 1C).

8. Frontal scour growth stops once a state of dynamic equilibrium is reached whereby sediment removal equals live-bed sediment inflowing. The maximum depth for this dynamic equilibrium is dependent on obstruction area facing the flow, median grain size, mean water velocity, and hydraulic pressure of water depth (Euler and others, 2017).

9. The open framework of the skulls used in the experiments allowed through-flow creating a more complex flow dynamics than flow around and over a bone (figures 6O, 9J, 9L, and 10G).

In the experiments with the beaver skull aligned perpendicular to flow, it immediately flipped onto its dorsal surface when flow was initiated (compare figure 11A with 11B). The reason for this is seen by the differential pressure fields on the upstream and downstream sides of the skull and the absence of through-flow (figure 11H). Although similar fields are developed with the other skulls, the small size of the skull made it particularly susceptible to the effects of the pressure gradient. The higher pressure on the upstream side sought to push the skull downstream, whereas the low-pressure zone on the downstream side sought to pull the skull
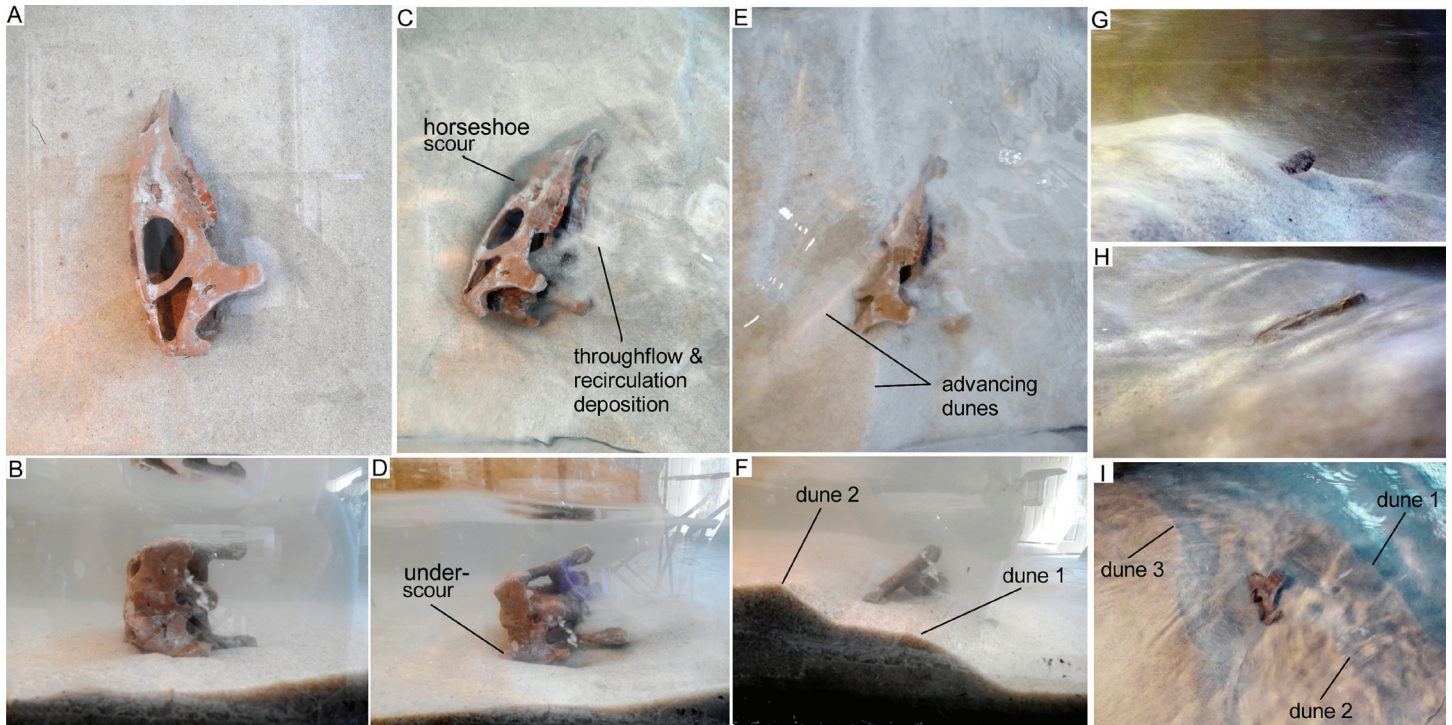
Figure 8. The effects of flow on a *Dryosaurus* skull cast resting on a live-bed. Conditions: sand (D_{60} = 0.35 mm, water depth = 30 cm, U= 0.5 m/s. Skull at start in (A) plan view and (B) underwater view of rear of skull. (C) Pivot of skull (about 42°) before scouring began. Scour and deposition co-occur; flow stopped for photography. (D) Upstream skull rotation into the horseshoe scour; compare with 8A and 8B; flow stopped for photography. (E) Burial by advancing dunes. (F) Side view showing burial by due to multiple dunes; flow stopped for photography. (G) Large dune about to bury protruding quadrate. White streaks and speckles are sand in suspension. (H) Start of exhumation of skull as sand dune passes; flow stopped for photography. (I) Skull about to be reburied (dune 3) after partial exhumation; flow stopped for photography.

in that direction. The net result of the push-pull forces on the skull was to flip it because tooth-bed resistance prevented the skull from merely sliding downstream.

Postcrania

Bones used included a cast cervical vertebra of *Camarasaurus* (figure 12), articulated dorsal and caudal vertebrae of *Varanus salvator* (figure 13), and femur of *Bos* (figures 5 and 14). Many of the same events with the skulls also occurred with the postcrania, such as the development of horseshoe scour on the upstream side, undercutting and sinking into the bed (figure 5F), and recirculation with deposition on the downstream side. The exception is the *Varanus* caudals as discussed separately below. With the rest of the postcrania, there were some notable differences from the skulls:

1. The deepest and largest scour occurred on the downstream side of vertebrae and femur aligned perpendicular to flow due to piping and lee side vortices (figures 12B, 13B, 13D, and 14B to 14F). Piping is due to the narrowness of bone-bed contact which allows higher seepage flow through porous sand, coupled with differential pressure on the upstream and downstream sides. This piping is similar to that seen with underwater pipes and horizontal cylinders, which leads to their self-burial (Chiew, 1990; Cataño-Lopera and García, 2006). Piping scour by its nature undercuts the bone on the downstream side because of fluidization of the bed, whereby water pressure forces the sediment upwards off the bed (figure 14G). The effects of piping is predicted to decrease the greater the mud content
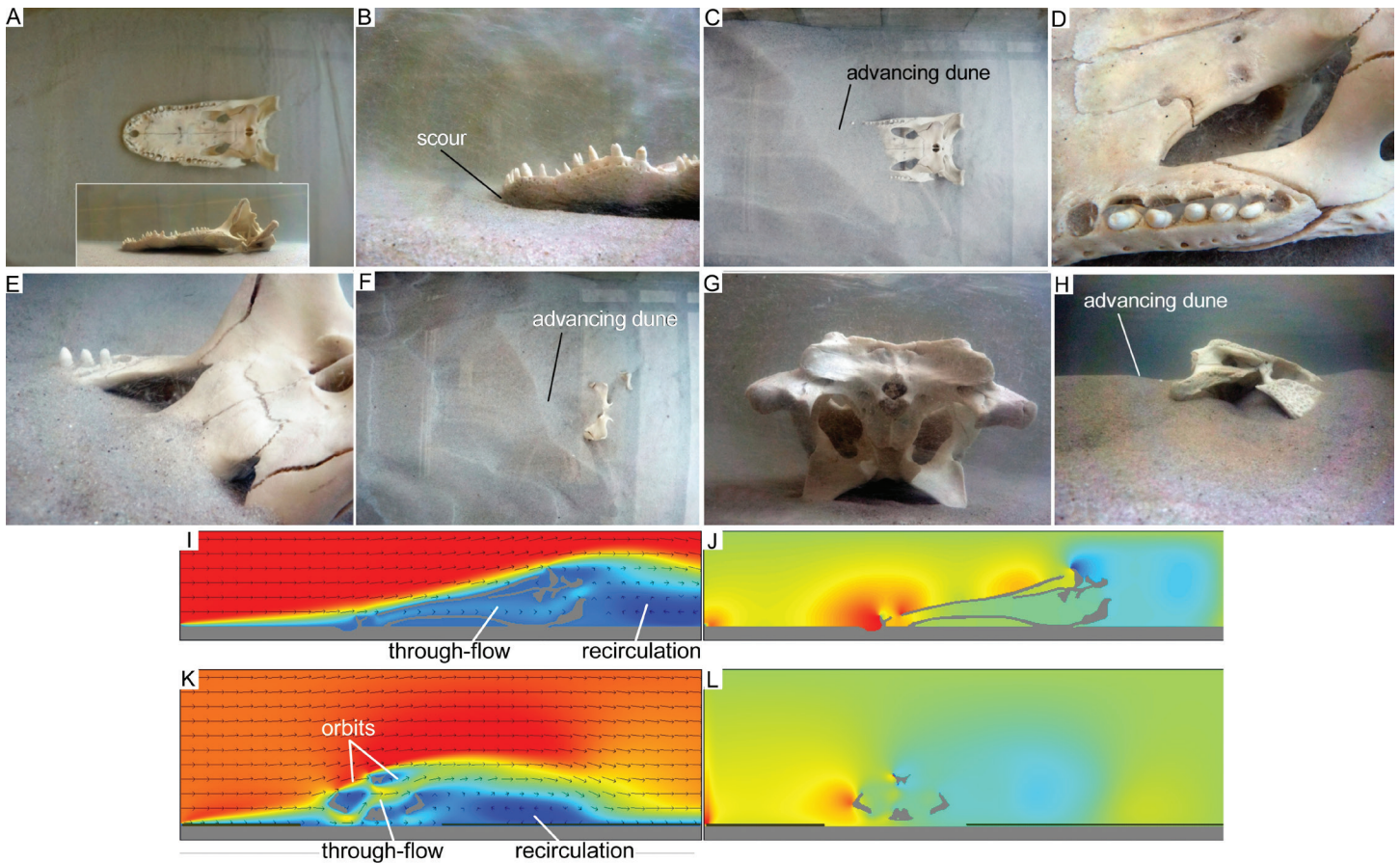
Figure 9. Effects of flow on an *Alligator* skull. Conditions: sand D_{60} = 0.35 mm, water depth = 30 cm, U = 0.5 m/s. (A) Skull at start in plan and side view. (B) Initiation of scour (white streaks are sand grains in suspension). (C) Burial by advancing dune; flow stopped for photography. (D) Sand grains being deposited within the skull. (E) Skull being infilled with sand cascading through the suborbital fenestra. (F) Skull nearly buried. Skull perpendicular to flow. (G) Skull at start from rear. (H) View upstream showing the burial by dunes. (I) CFD showing flow velocity fields (U = 0.5 m/s) through skull aligned with flow. The low velocity through-flow explains deposition of sand grains within the skull seen in 9D. Blue = 0.026 m/s, red = 1.087 m/s. (J) CFD of pressure showing high-pressure at the tip of the snout where scour is seen in 9B. Peak pressure 3203 Pa. Note lower pressure within most of the skull. (K) CFD showing complex flow velocity fields (u = 0.5 m/s) though the rear portion of the skull set perpendicular to flow. Blue 0.00297 m/s; yellow = 0.495 m/s; red 1.287 m/s. (L) CFD pressure gradients of 9K with peak at 1125 Pa.

of the substrate due to reduction in pore space.

2. Non-piping, lee side scouring occurs if the approaching velocity is high enough to cause flow over the bone to reach supercritical velocity due to hydrostatic pressure of the water column ("thumb on the garden hose" effect). It then swoops down behind the bone in a jet-like motion to scour the bed (figure 14G). This effect is similar to the stratified flow hydraulic jump described by Dorrell and others (2016).

3. Once the scour hole is formed, the bone rotates downstream into the scour hole (figures 12B and 14C to 14F). This movement is assisted by high flow pressure on the upstream side and low-pressure wake vortex on the downstream side (figure 14H). Piping and scour can also cause a bone to sink into the bed with minimal downstream rotation, especially if the bone is relatively narrow and with a low profile (figures 14J and 14K).

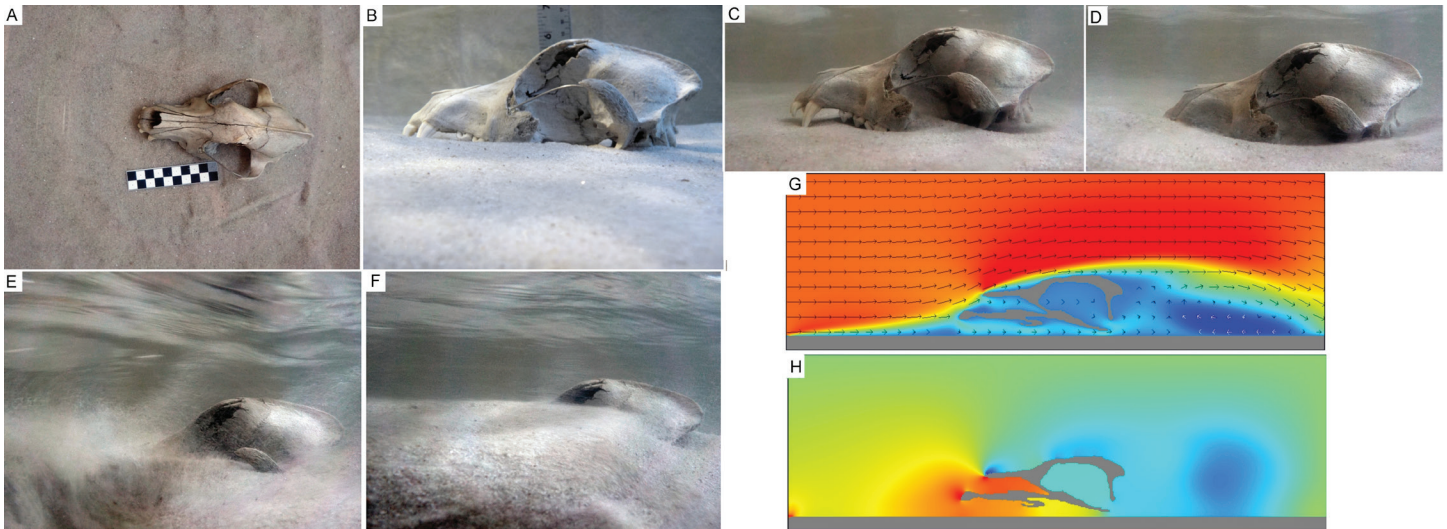The *Varanus* caudal section behaved different from

Figure 10. Effects of flow on a modern dog skull aligned with flow presenting a minimal profile. Conditions: sand D_{60} = 0.35 mm, water depth = 30 cm, U = 0.5 m/s. (A) Skull in plan view. (B) Skull in side view. Note the canines hold the palate off the bed. (C) Under scour causes the rear part of the skull to sink into the bed; flow stopped for photography. (D) Maximum self-burial of skull prior to burial by advancing dune. (E) Recirculating flow along lee side of advancing dune (U = 1 m/s). (F) Near burial by dune (U = 1 m/s); flow stopped for photography. (G) CFD flow velocity fields (U = 0.5 m/s). Blue = 0.00394 m/s; yellow = 0.497 m/s; red = 1.274 m/s. (H) CFD of pressure gradients; note higher pressure beneath the skull, exactly where scour occurs in 10C causing the skull to sink. Pressure beneath the skull about 1563 Pa.

the other postcranial elements and is discussed separately. When the caudal ribs were pressed into the bed, they acted as anchors and scour developed as with the skulls. In contrast, when the caudal vertebrae were supported by the chevrons and caudal ribs (figures 13G and 13H), through flow beneath the centra prevented the buildup of pressure on the upstream size and no scour developed. Burial was strictly by bed migration.

Live Bed Phase

In these experiments, scour alone was insufficient for bone burial because scour-hole depth never exceeded bone height. Tilting of the bone into the scour hole reduces its profile in the flow, thereby reducing both the downwelling and effective scour energy. Eventually, a point of dynamic equilibrium is reached at which no further deepening of the scour occurred, generally between half to three-quarter bone height and is dependent on the approaching mean flow velocity. This phenomenon of equilibrium has been noted in other scour studies (Euler and Herget, 2012; Friedrichs and others, 2016; Euler and others, 2017).

Complete burial of skulls and postcrania is due to migrating bed forms (figures 6J to 6L, 7D, 7E, 8E to 8G, 9C, 9F, 9I, 10E, 10F, and 11C), with several events occurring:

1. Downstream deposition of turbulent sand suspension from the crest of an approaching dune due to vortex shedding in the separation zone where peak velocity occurs (figures 2B, 4B, 4C, and 8G; Kostaschuk and Villard, 1999; Best, 2005). Entrained sand grains in the recirculation zone then settled on the bone once flow velocity dropped below the transport threshold (figures 6H and 6I). Although a minor cause of burial by sand compared to burial by the dune itself, this downstream deposition was found to increase as the dune approached and the dune flow shadow enveloped the bone.

2. Because flow deceleration occurs on the lee side of dunes (Best, 2005), bed erosion in the vicinity of the bone gradually slows and eventually halts, then infills from cascading sand from the dune slip-face (compare figure 6F with 6J, and 6K).
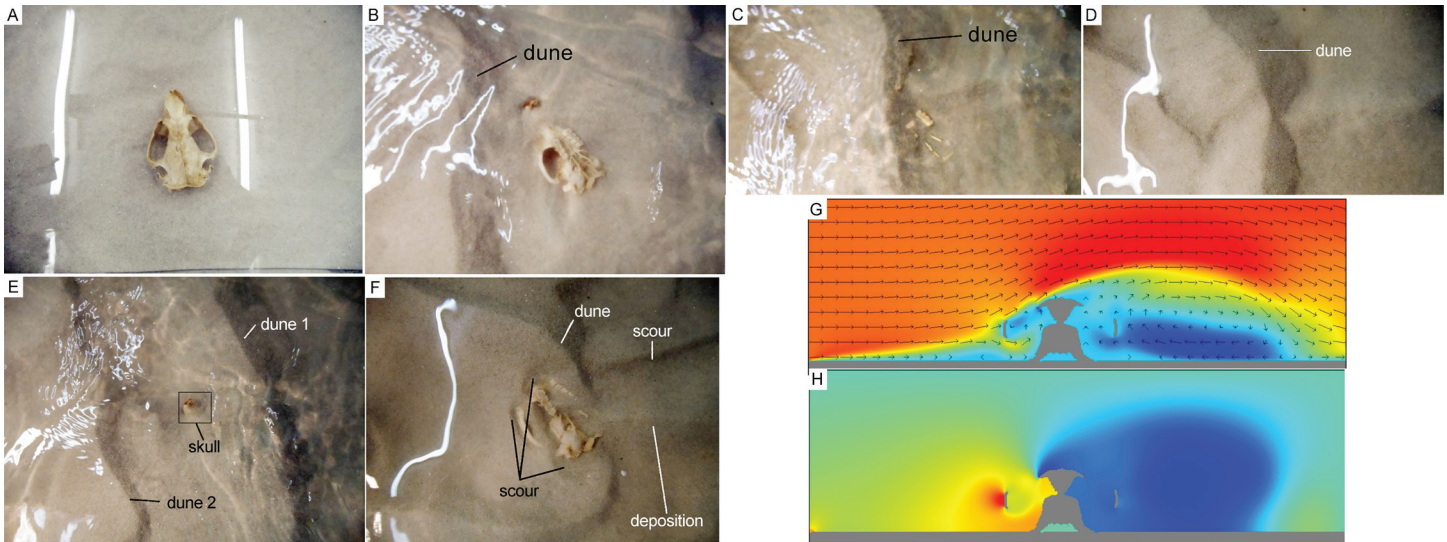
Figure 11. Effects of flow on modern beaver skull perpendicular to flow, with repeated burial and exhumation. Conditions: sand D_{60} = 0.35 mm, water depth = 30 cm, U = 0.5 m/s. (A) Skull at start. (B) Skull was immediately flipped over. Advancing dunes of live bed start burying the skull; flow stopped for photography. (C) Skull nearly completely buried. (D) Skull completely buried; flow stopped for photograph. (E) Start of exhumation as dune moves. (F) Maximum exhumation; flow stopped for photography. (G) CDF of flow velocity around skull. Blue = 0.00565 m/s; yellow = 0.3983 m/s; red = 1.332 m/s. (H) CDF of pressure gradients showing high pressure (red to yellow) on the upstream side of the skull and large area of low pressure (blue) on the downstream side. This differential pressure explains why the skull flipped over. Peak pressure = 1406 Pa.

3. Once the dune begins to envelope the bone, cascading sand infills open voids within bone and skulls, except for dead end pockets that face upwards (figures 9D and 9E). Currents flowing down the lee side of the dune may also push sand grains into voids.

4. Further advancement of the dune completely covers the bone (figures 8F, 8G, 9F, and 11B to 11D), unless the bone height exceeds dune height (figure 10F).

5. Continued downstream migration of the dune may exhume the bone (figures 8G, 8H, and 11C to 11F), then it may be reburied by the next advancing dune. This cycle can occur repeatedly subjecting the bone to abrasion by approaching saltating grains (Thompson and others, 2011; Griffith and others, 2016) that may mimic bone transport abrasion (Shipman and Rose, 1988; Andrews, 1995; Fernández-Jalvo and Andrews, 2003), but this abrasion is not uniform over the bone. Permanent burial occurs in aggrading channels, but even so, the rate of aggradation will be less than the rate of dune migration. This implies that a cycle of burial and exhumation is part of the normal process of bone burial.

CONCLUSION OF FLUME STUDIES

Bone burial in an aggrading fluvial channel is not a simple process of sand being transported and deposited over the bone. Rather, the bone sets up the initial condition for its burial. This point was also noted by Johnson's (1957) study of shells in a flume; however, the study did not explain the hydraulic effects that took place. Bones disrupting flow causing a U or horseshoe vortex that scours the bed along the entire upstream side. The scour may extend beneath the bone as well and if this undercutting extends to more than half the bone width (as measured in the X axis, the direction of flow), the bone may tilt into the scour hole. This event in unidirectional flow is seldom sufficient to completely lower the bone below the bed surface. In contrast, scour may be the primary method for burial when the object is subjected to oscillatory flow because of under scour on both side of
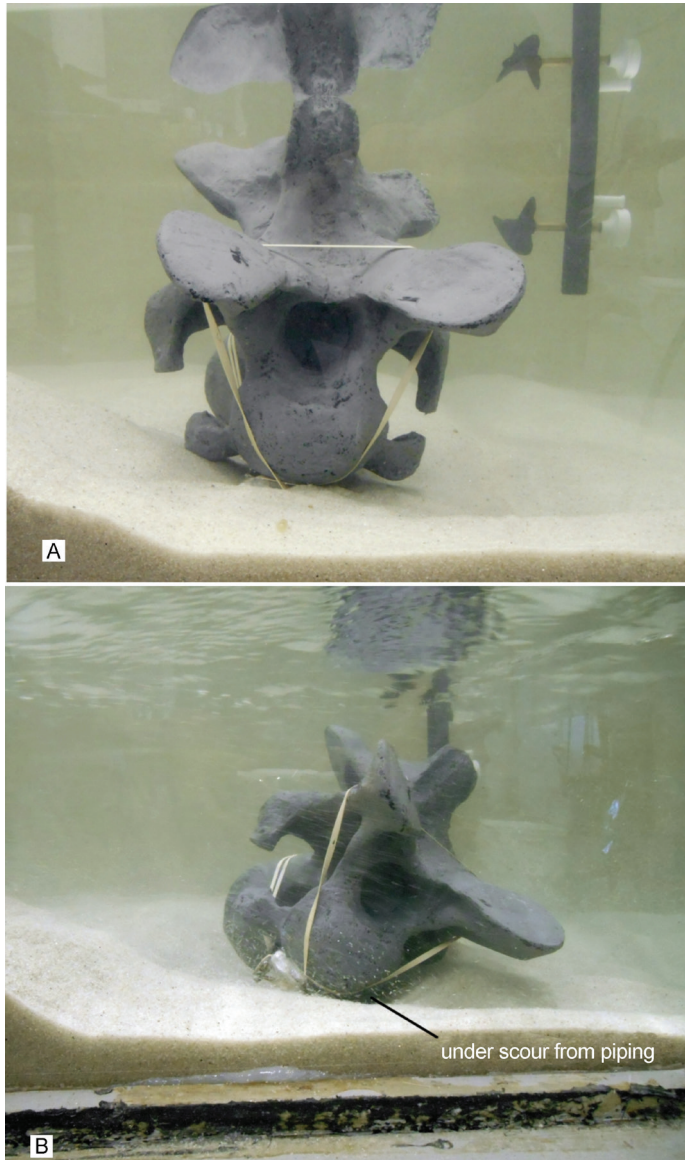
Figure 12. Effects of under scouring piping on a vertebra. (A) Cervical vertebra (*Camarasaurus*) cast at start of experiment, dune to the left. (B) Downstream rotation after scour from piping and force of flow deflected over the dune at the far left.

the obstruction (Dill, 1958; Cataño-Lopera and García, 2006).

The process of burial occurs when flow velocity drops below the critical threshold for grain transport. This generally occurs first in the localized recirculation zones of flow shadows of complex bone shapes due to form drag and flow separation. These localized recirculation zones may also develop where through-flow passes into the unconstrained downstream side of var-

ious skull openings. Cascading sand on the lee side of approaching dunes infills bone voids, but this may be hampered by soft tissue. Once decay has removed the tissue, then sand, if not lithified, is predicted to infill much of the void from fluidized sand injection by overpressure. Primary voids in fossil skulls (Daniel, 2012) demonstrate that infilling is not always complete. Advancement of the dune eventually envelops the bone and if the bone is less than the dune height, it will be completely buried. Continued migration of the dune may exhume the bone as the sand moves downstream. However, subsequent dune migration cyclically buries and exposes the bone. We may predict that only in aggrading river channels is burial eventually permanent.

USING FLUME MODELING TO INTERPRET A BONE BED

The different flume bone burial experiments described above show repeated patterns regardless of bone size and shape suggesting underlying principles at work summarized in the previous section. This raises the question whether the results can elucidate events that led to the burial of bones in an actual fossil bone deposit. This hypothesis is explored using the bone bed in the Morrison Formation at the quarry visitor center at Dinosaur National Monument, Utah. The bones at the quarry occur in fluvial channel sandstones (Holland, 1915; Gilmore, 1936; Bilbey, 1973; Bilbey and others, 1974; Lawton, 1976, 1977; Turner and Peterson, 1992; Fiorillo, 1994; Foster, 2003; Carpenter, 2013), and most probably represent a braided river complex (Lawton, 1976, 1977; Carpenter, 2013). The recent crevasse splay hypothesis of Brezinski and Kollar (2018) is doubtful because: (1) the conglomeratic quarry sandstone (larger clast sizes 2–10 cm) is in contrast to the generally coarse sand- to fine- sand of crevasses splays (Millard and others, 2017), (2) the healing of the crevasse that would result from the abrupt decrease in competence, and specifically the conglomeratic-coarse sand carrying capacity as part of the river flow was diverted out of channel (Nienhuis and others, 2018), (3) the difficulty in transporting large clasts with masses in the high tens of kilogram (e.g., sauropod bones) by rapidly decelerating water of a splay (these should also accumulate at
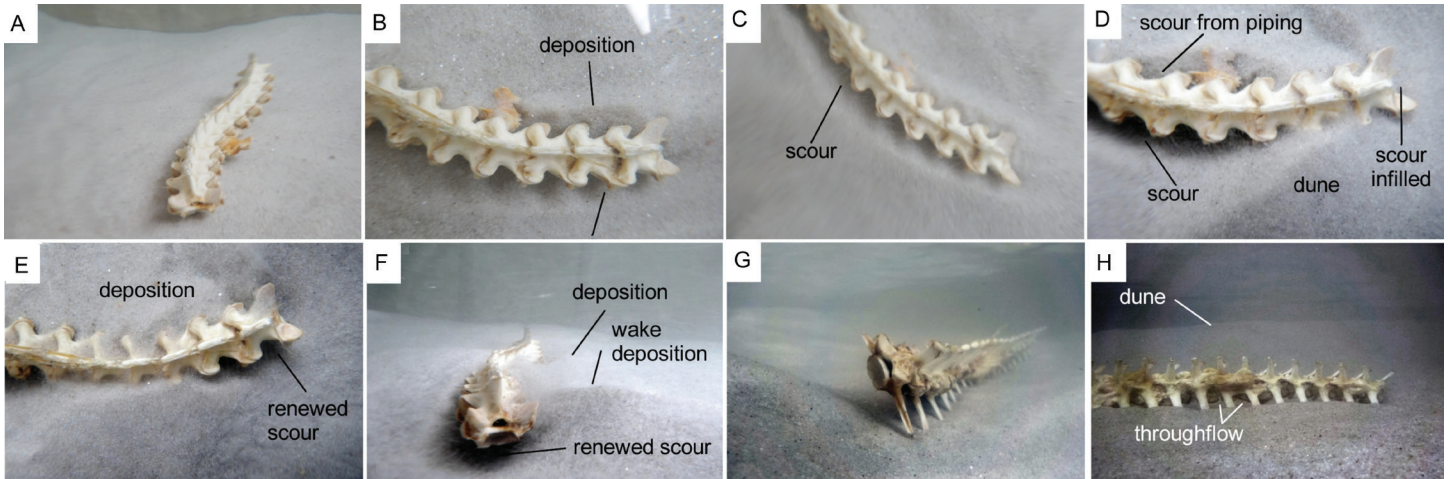
Figure 13. The effects of flow on an articulated string of *Varanus* vertebrae. Conditions: sand D_{60} = 0.35 mm, water depth = 30 cm, U = 0.5 m/s. (A) Oblique view of vertebrae perpendicular to flow at start. (B) Scour upstream side and deposition on downstream side from underflow. (C) Scour along the entire upstream side. (D) Scour from piping and advancing dune, which shut off and then buried the scour. (E) After the advance of the dune, there is renewed scour. (F) Front (end) view of E showing the under scour. (G) Articulated caudal vertebrae supported by the chevrons and transverse processes at start. (H) Upstream view showing advancing dune. Little scour occurred because flow could pass under the vertebrae.

the mouth of the crevasse channel causing blockage and healing; see #2), (4) dinosaur bones are known to act as sediment traps because of frictional flow resistance (form drag) and turbulent eddies from flow separation causing a velocity drop and an loss of sediment transport competence (figure 15), (5) related to #4 are that the bone jams are analogous to boulder arrays, which are known to bear a significant component of bed shear stress, thereby reducing the available shear stress available for sediment transport (Papanicolaou and others, 2012), and (6) the difficulty of accounting for the enormous volume of water at supercritical flow needed to move large dinosaur bones of the 1.8-km-wide conglomeratic splay hypothesized by Brezinski and Kollar (2018) in a semiarid environment. These and other issues are dealt with elsewhere (Carpenter, in preparation).

Bed forms responsible for bone burial are well displayed either in historical photographs (see figure 13 in Carpenter, 2013) or currently on the bone wall. These bed forms include channel bars (figure 16A), dunes and planar cross-beds of dunes (see figure 26 in Carpenter, 2013). These planar cross-beds show the coarsening upwards and fining towards the toe that is characteristic

of high sediment transport rate (Bridge, 2003). These bed forms can be shown to have buried the bones as discussed below.

Some of the features generated by the bone obstacles in the flume experiments are observed on the quarry. Scour is perhaps the most obvious paleo-event observed, especially the downward displacement of the ends of articulated vertebrae strings explained as due to the horseshoe scour extending around the edge of the obstacle and pliable ligaments (figure 16B). Scour evidence is also seen by bones angled in the upstream direction of the paleoflow, with the downstream side higher than the upstream side (figure 16C). This angling is similar to that seen by the upstream helical undercutting and tilting of bone. The effects of flow on one moderate-sized scapula-coracoid was even more extreme because the bone stands almost vertical in the sediments (figure 16D). This is interpreted to have been caused by undercutting along the anatomical dorsal margin, which faced upstream, and subsequent tilting and renewed under cutting. No large scapula-coracoids show such extreme tilting probably because their large (relative to stream flow) size prevented renewed under scour after the tilting. Not all bones show evidence of
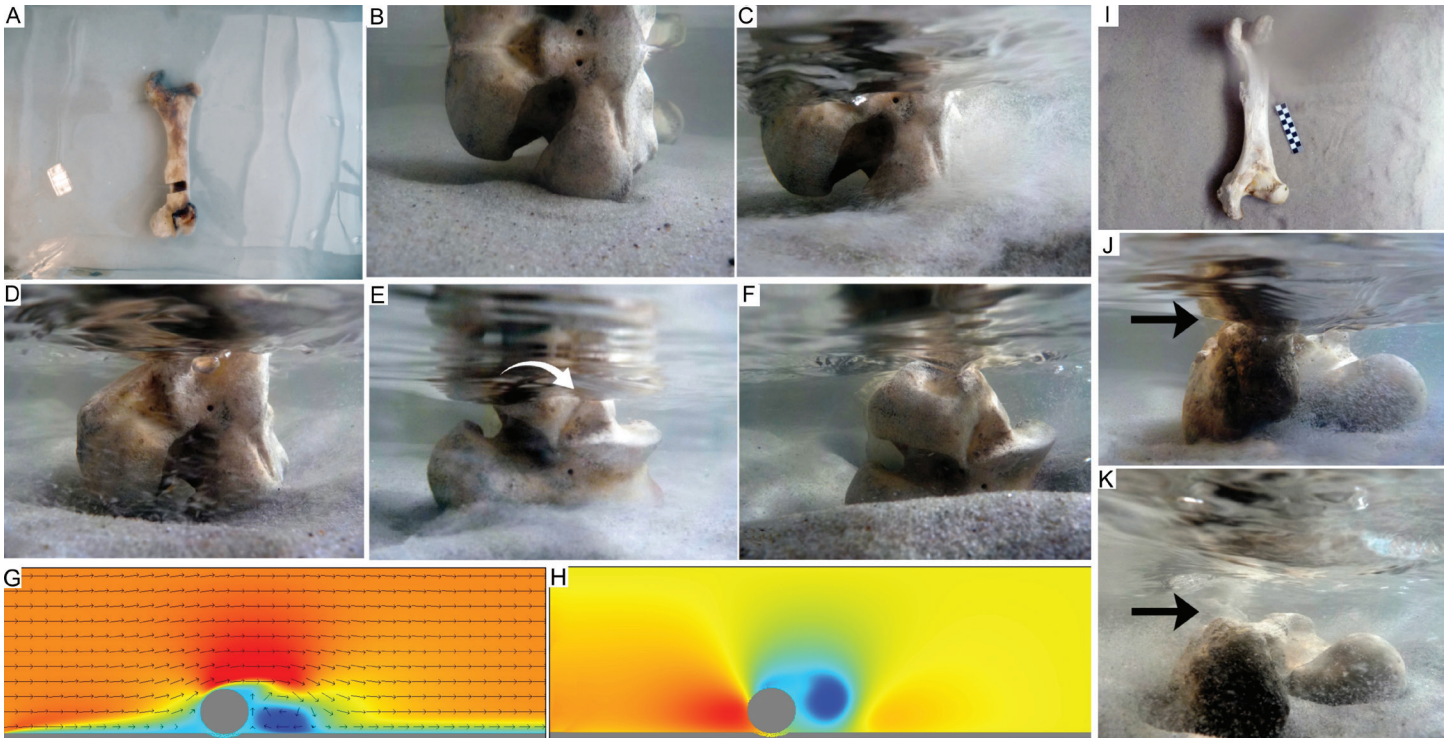
Figure 14. Effects of flow on a domestic cow femur. Conditions: sand D_{60} = 0.35 mm, water depth = 30 cm, U = 0.5 m/s. (A) Femur at start aligned perpendicular to flow. (B) Distal end showing condyles only half underwater. (C) Scour beginning at distal condyle (cloudiness due to sand particles in suspension). (D) Femur begins to sink into bed scour; note more of the condyles submerged. (E) Being more submerged increased surface area subjected to flow resulting in femur rotating downstream. (F) Continued scouring lead to partial burial of femur. (G) CFD showing flow velocity fields (U = 0.5 m/s). Blue = 0.0060 m/s; yellow = 0.413 m/s; red= 1.432 m/s. (H) CFD showing differential pressure gradients of (G) to explain why the femur rotated in (E); red is high pressure zone; blue is lowest pressure. (I) Femur inverted to a more stable position seen in plan view aligned perpendicular to flow. (J) Proximal end seen underwater. Arrow draws attention to the bone just contacting the surface. (K) Scour has resulted in the bone sinking into the bed. Arrow denotes gap between bone and surface.

undercutting and these are typically elongate and parallel with paleoflow. Because undercutting scour must extend more than 50% for the bone to tilt into the scour hole, these elongated bones never experienced that amount of scour before burial so remained horizontal on the substrate (figure 16E). However, elongate bones not parallel to flow or which were subjected to more than 50% under cutting do slope upstream (figure 16F).

Evidence for wake scour and fill is best seen where finer grain sand infilled the scour around the sides and downstream of the bone (figure 17A). A helical scour hole near the front edge of a vertebra may have infilled with fine-grained sand when the force of the flow decreased with the proximity of an approaching bed form (figure 17B). Through or underflow and scour are seen

with the coosified *Stegosaurus* sacrum and ilia (presumably without the pubes and ischia). The infilling is with fine-grained sand (figures 17C and 17D). A pocket of gravel (figure 17D) may be lag from winnowing of the bed by the underflow. Overflow of a low-profile bone results in the formation of a low-pressure recirculation zone on the lee side of the bone (e.g., figure 17 G) resulting in the deposition of fine-grained sediment (figure 17E), as well as smaller bones (figure 17F).

One peculiar burial is an immature *Diplodocus* pelvis oriented perpendicular to the sediments, anterior side down (figures 18A to 18C). The most parsimonious explanation in light of this study, is that the pelvis somehow got into a stable vertical position where it was soon enveloped by a migrating bar or megadune, which

Figure 15. Example of a bone bed that acted as a sediment trap to crevasse splay sands. Splay sandstone in the foreground rapidly thins towards the back and ends approximately at red line. Beyond that bones lie in sandy mudstone. Note femur in foreground that cuts obliquely through sandstone due to original scouring of upstream end (nearest viewer). Children's Museum of Indianapolis excavation, Morrison Formation, Big Horn Basin, Wyoming.

is represented today by "the Hump" on the quarry face (figure 16A; Carpenter, 2013). There is a large portion of what may be the rest of the skeleton exposed on the west side of "the Hump" but these bones are lying horizontally.

One skull remaining on the bone wall ("cliff face" skull) shows the effects of paleoflow, which resulted in its slight displacement from the articulated cervical vertebrae (figures 18D and 18E). Sauropods are notorious for the rarity of their skulls being found with the skeleton and this specimen suggests that the muscles and lig-

aments attaching the vertebral column to the skull decompose rapidly. The cervical vertebrae are ventral-side up, whereas the skull lies on its left side, implying that originally there must have been considerable torsion stress at the skull-neck junction. Eventually, the stress on the decay-weakened joint separated the skull, possibly aided by the force of the water. The skull was then pushed along the bed several centimeters. Decay also affected the connective tissue of the joints on the upside (right side) of the skull. The liberated right quadrate, quadratojugal, and some of the palatal elements were gravitationally displaced towards the downside of the skull. The articulated dentary, surangular, and angular, and the disarticulated prearticular, splenial, and many of the teeth of the right mandible were displaced downstream a little from the skull (Madsen and others, 1995). This evidence for the decay of almost all of the soft tissue allowed sand to cascade into and fill the inside of the skull (compare with figure 9E). Because clay-poor (<10%) siliciclastic sediment with grain-to-grain contact has long been known to resist mechanical compaction from postdepositional overpressure (e.g., Athy, 1930; Weller, 1959), the lack of crushing of the skull indicates that all the major cranial voids (e.g., brain cavity and snout) were supported by sand grains. This contrasts with skulls from clay-rich sandstone or skulls still encased in soft tissue at the time of burial; these skulls show compaction crushing (Carpenter, 2013).

CONCLUSIONS

Laboratory water flumes have played an important role in our understanding of fluvial systems using controlled and repeatable experiments to understand hydrological processes. Laboratory flumes have also been used to understand bone sorting and transport, which has been important in understanding taphonomic bias observed in fossil deposits. This study used a laboratory flume to study the next phase, bone burial under controlled conditions. The bones used, real and cast, replicate many of the features documented for bed obstacles (e.g., Martinuzzi and Tropea, 1993; Istiarto, 2001; Smith and Foster, 2007; Dey and others, 2008; Euler and Herget, 2011; Mazumder and others, 2011), including turbulent flow features also seen around obstacles (e.g.,
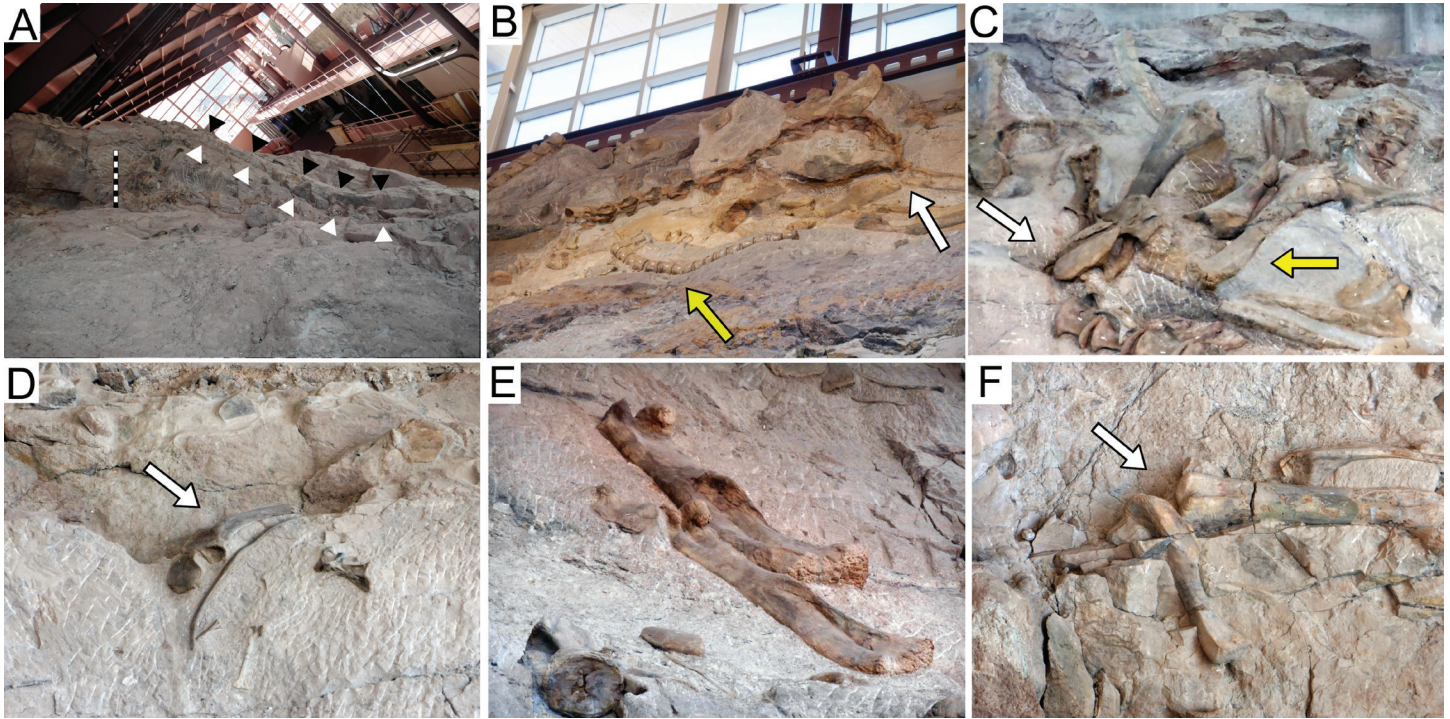
Figure 16. Bone wall inside the Quarry Exhibit Hall at Dinosaur National Monument. (A) Inclined strata of a channel bar preserved on "the Hump" at the west end of the Carnegie Quarry. Flow was left to right. Scale approximately 1 m; the pelvis in figure 18 is immediately to the right of the scale. (B) Evidence of scour at the end of the diplodocid cervical vertebrae (white arrow), and possible pipping erosion + underflow scour (yellow arrow). (C) Arrows point to the lower end of bones at an oblique angle through the strata due to scour; *Diplodocus* anterior caudal (white arrow), diplodocid humerus (yellow arrow). (D) Sauropod scapula (arrow) dipping upstream due to scour. (E) Lack of apparent under scour seen with two long sauropod femora (lower *Diplodocus*; upper *Apatosaurus*) lying flat on bedding surface. (F) Two long bones (arrow; humerus, left; femur, right) oblique to strata due to under scour. Unless stated otherwise, average flow direction was from the top of image.

Euler and Herget, 2012; Euler and others, 2017). Therefore, bones are governed by the same hydraulic principles (i.e., similitude) and can be reliably modeled in a flume and by computational fluid dynamics.

The bones in the flume showed the following generalities, with no marked difference between the fine (D_{60} 0.35 mm) and coarse (D_{60} of 0.9 mm) grain bed loads:

1. Along the upstream side, the constant approach of water causes down flow and development of a horseshoe-shaped helical vortex as the water seeks to escape around the bone margins into regions of lower pressure.

2. Depending on how deep into the bed substrate the bone rests, under scour can develop along the upstream edge. If this scour extends to greater than half the bone length, the bone can tip upstream into the scour hole and lay at an angle to the strata. This suggests caution for interpreting low angled (30°) fossil bones in sand-rich sedimentary rock as indicative of trampling.

3. Underflow can also cause scour beneath the bone where the water is constricted beneath any irregularly shaped bone in which a part maybe slightly elevated above the bed.

4. The erosive strength of the down flow along the upstream side is reduced when the bone has a streamlined frontal area because the flow is more easily deflected around the bone.

5. Under scour can develop from piping due to hydrostatic pressure on the upstream side forcing sand up off the bed on the downstream side, but this seems to be confined to vertebrae laying perpendicular to flow. Presumably, pipping can
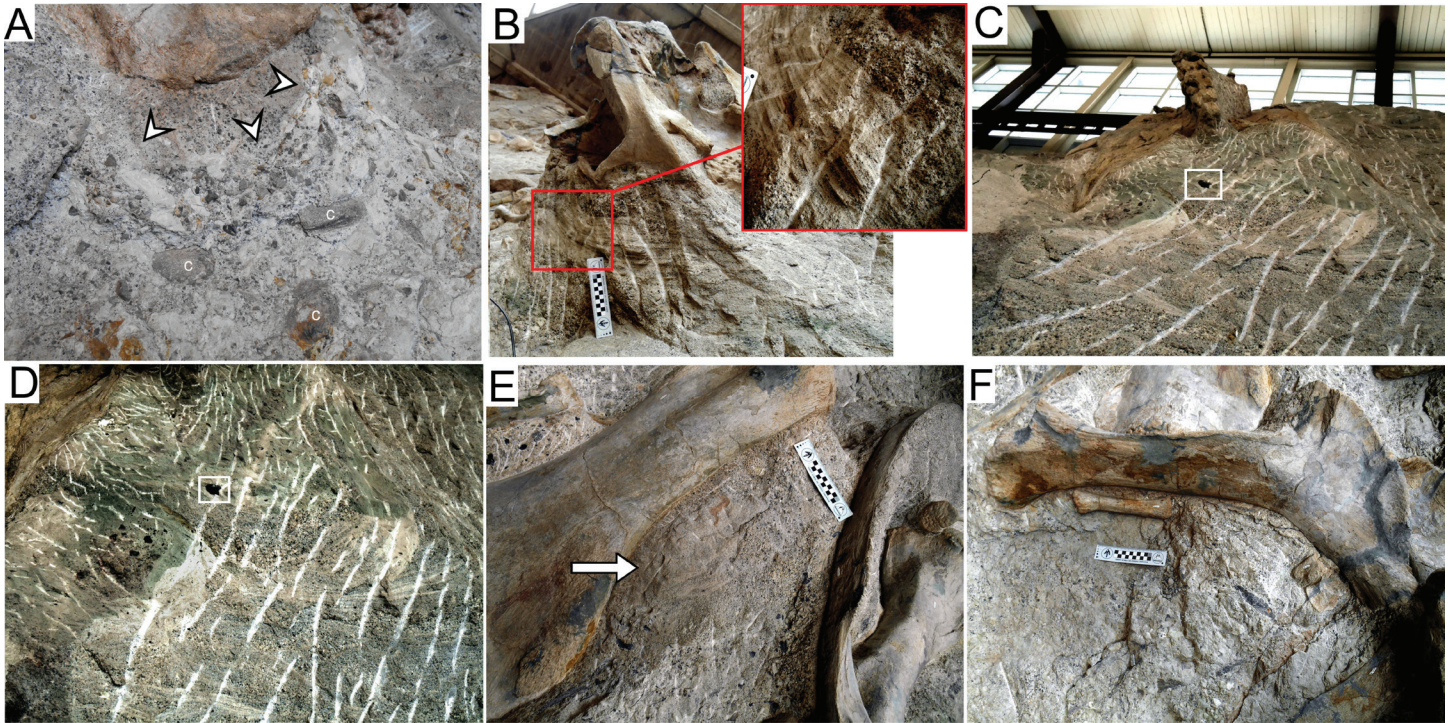
Figure 17. Bone wall inside the Quarry Exhibit Hall at Dinosaur National Monument. (A) Downstream scour from wake vortices and later infill (darts) around bone obstacle. Note bone was at slight angle relative to flow resulting in more pronounced scour on right side. Clam (c) valves came to rest in stable position in flow shadow. (B) Fine-grained fill of the scour formed by the helical vortex along the front edge of the obstacle (diplodocid vertebra). Inset shows detail. (C) Partial *Stegosaurus* pelvis oriented parallel with current with scour and fill structures downstream (lighter lenses). White box is landmark in (D). White streaks caused by excavation tools. (D) Detail of scour from underflow of *Stegosaurus* sacrum and ilia and with lag and later infill. White box is landmark in (C). White streaks caused by excavation tools. (E) Fine-grained sand deposited in the flow shadow side of a diplodocid sauropod humerus; note coarser sand farther downstream (lower right). (F) Small bone (ulna) and other small bones in the flow shadow side of a sauropod (*Diplodocus*) ischium (note also the finer grained sandstone).

also occur with ribs or other slender bones presenting a narrow cross section to flow.

6. As the water passes over or around the bone, flow deceleration and separation occurs forming recirculation eddies on the downstream side. Recirculation is in a lower pressure gradient causing deposition of sediment, part of which is derived from the frontal scour. This lower pressure is the result of a rapid change from constricted to unconstricted flow. The drop in velocity causes a loss in the transport capacity, with a net gain in sedimentation.

Despite some bones partially setting up the conditions for their own burial through settling into a scour hole or acting as sediment traps, the main cause of burial is by migrating bed forms.

The results of the flume experiments do explain some of what is seen on the bone wall at Dinosaur National Monument, and suggests the generalized results have a broader applicability with other fossil bone deposits as well. However, this study only investigated the processes of burial for bones resting on a sandy, clay-poor substrate. The effects of interstitial binding agents (clay or microbial mats) to resist bed erosion were not considered. These agents are known to hinder scouring until the critical velocity of the sediment is surpassed (Paterson, 1994; Droppo and others, 2015; the so-called "stick 'n' peel" of Orr and others, 2016, may not hold for sandy beds).

Future investigation should examine flow around single bones using 3-D computation fluid dynamic
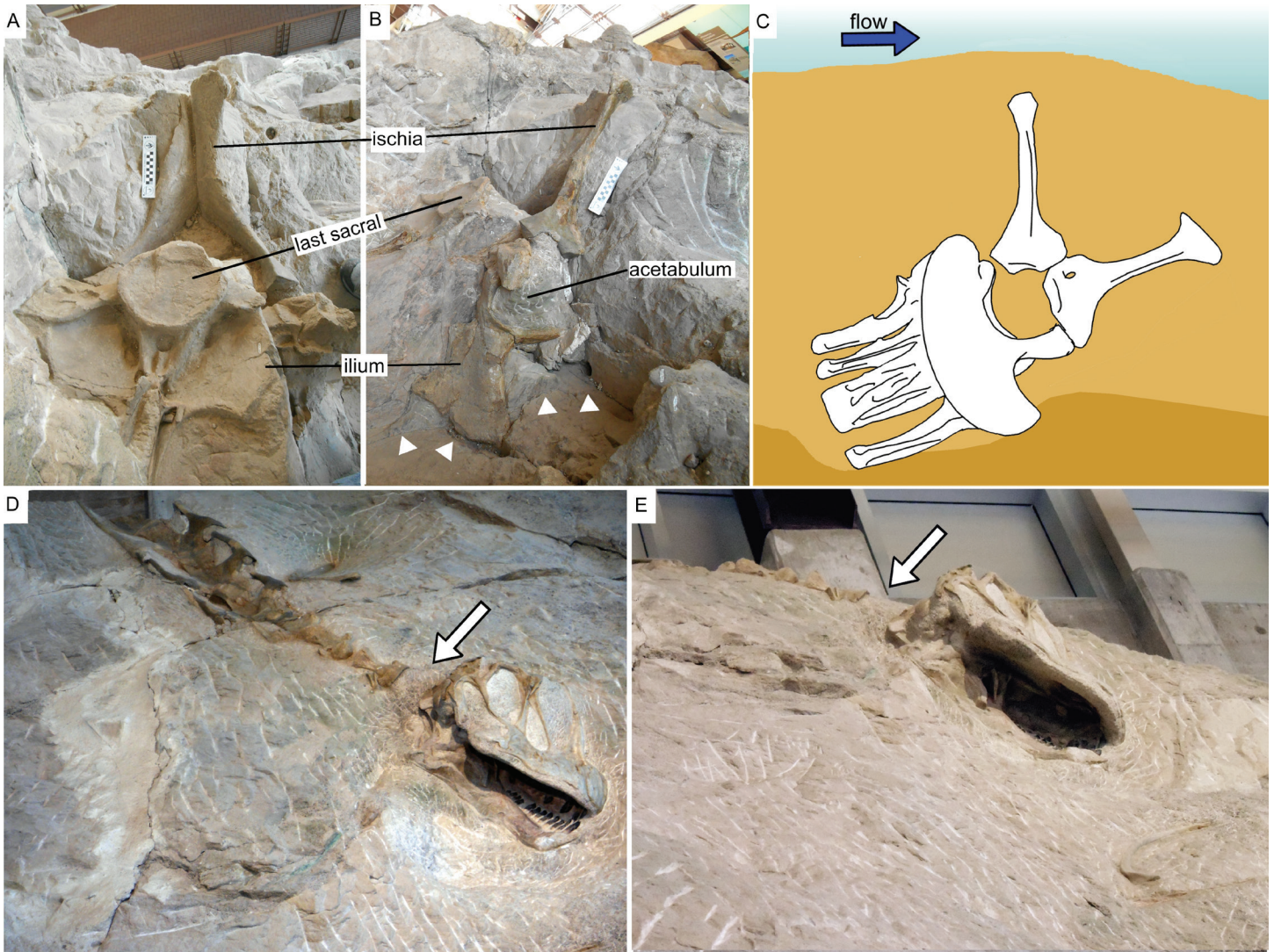
Figure 18. Bone wall inside the Quarry Exhibit Hall at Dinosaur National Monument. (A) End view of posterior side of sauropod pelvis (*Diplodocus*) standing vertically through bar deposit. (B) Side view of sauropod pelvis at "the Hump." Darts indicate a lithological boundary that may represent a bed surface. (C) Interpretative sketch. (D) Anterior cervical vertebrae and slightly displaced skull of *Camarasaurus*. (E) Palatal view showing that the skull is not crushed and infilled with sandstone. White arrows indicate separation of skull from cervical vertebrae.

software with a variety of grain sizes in a moveable bed. This should provide a refined understanding of bones as obstacles and an understanding of bone burial. In addition, scour hole geometry is known to be influenced by the angle of the obstruction to the flow (Johnson, 1957; Haltigin and others, 2007), but this was only partially examined in this set of experiments (e.g., alligator and dog skulls). Scour is also known to occur at the confluence on the downstream side of bars (Ashmore and Parker, 1983; Szupiany and others, 2019) and this is predicted to influence bone burial. Finally, modeling of carcasses and partial carcasses also remain an important area for future exploration.

ACKNOWLEDGMENTS

view comments to earlier versions by three anonymous reviewers, Susannah Maidment (Natural History Museum, London), Patrick Orr (Department of Geology, National University of Ireland), and Kathleen Huber (Paleontological Society) are gratefully acknowledged. This article is the seventh in a series on Dinosaur National Monument.

REFERENCES

Andrews, P., 1995, Experiments in taphonomy: Journal of Archaeological Science, v. 22, no. 2, p. 147–153.

Ashmore, P., and Parker, G., 1983, Confluence scour in coarse braided streams: Water Resources Research, v. 19, p. 392–402.

Athy, L.F., 1930, Density, porosity, and compaction of sedimentary rocks: American Association of Petroleum Geologists Bulletin, v. 14, p. 1–24.

Best, J., 2005, Kinematics, topology and significance of dune-related macroturbulence—some observations from the laboratory and field, *in* Blum, M.D., Marriott, S.B., and Leclair S.F., editors, Fluvial sedimentology VII: International Association of Sedimentologists Special Publication 35, p. 41–60.

Bilbey, S.A., 1973, Petrology and geochemistry of the Morrison Formation, Dinosaur Quarry quadrangle, Utah: Logan, Utah State University, M.S. thesis, 102 p.

Bilbey, S.A., Kerns, R.L., and Bowman, J.T., 1974, Petrology of the Morrison Formation, Dinosaur Quarry quadrangle, Utah: Utah Geological and Mineral Survey Special Studies 48, p. 1–15.

Biron, P.M., Robson, C., Lapointe, M.F., and Gaskin, S.J., 2005, Three-dimensional flow dynamics around deflectors: River Research and Applications, v. 21, p. 961–975.

Blob, R.W., 1997, Relative hydrodynamic dispersal potentials of soft-shelled turtle elements—implications for interpreting skeletal sorting in assemblages of non-mammalian terrestrial vertebrates: Palaios, v. 12, p. 151–164.

Blöschl, G., and Sivapalan, M., 1995, Scale issues in hydrological modelling—a review: Hydrological Processes, v. 9, p. 251–290.

Boaz, D.D., 1982, Modern riverine taphonomy—its relevance to the interpretation of Plio-Pleistocene hominid paleoecology in the Omo Basin, Ethiopia: Berkeley, University of California, Ph.D. dissertation, 376 p.

Boaz, N.T., and Behrensmeyer, A.K., 1976, Hominid taphonomy—transport of human skeletal parts in an artificial fluviatile environment: American Journal of Physical Anthropology, v. 45, p. 53–60.

Bocchiola, D., 2011, Hydraulic characteristics and habitat suitability in presence of woody debris—a flume experiment: Advances in Water Resources, v. 34, p. 1304–1319.

Bocchiola, D., Rulli, M.C., and Rosso, R., 2008, A flume experiment on the formation of wood jams in rivers: Water Resources Research, v. 44, p. 1–17.

Brezinski, D.K., and Kollar, A.D., 2018, Origin of the Carnegie Quarry sandstone (Morrison Formation, Jurassic) at Dinosaur National Monument, Jensen, Utah: Palaios, v. 33, p. 94–105.

Bridge, J.S., 2003, Rivers and floodplains—forms, processes, and sedimentary record: Oxford, Blackwell Publishing, 491 p.

Brørs, B., 1999, Numerical modeling of flow and scour at pipelines: Journal of Hydraulic Engineering, v. 125, p. 511–523.

Carpenter, K., 2013, History, sedimentology, and taphonomy of the Carnegie Quarry, Dinosaur National Monument: Annals of Carnegie Museum, v. 81, p. 153–232.

Carpenter, K., 2016, After the bone moves—actualistic experiments and computational fluid dynamics on stationary bone in a water flume [abs.]: Society of Vertebrate Paleontology 76th Annual Meeting Program and Abstracts, p. 110.

Carpenter, K., 2018, Rocky start of Dinosaur National Monument (USA), the world's first dinosaur geoconservation site: Geoconservation Research, v. 1, p. 1–20.

Carré, D.M., Biron, P.M., and Gaskin, S.J., 2007, Flow dynamics and bedload sediment transport around paired deflectors for fish habitat enhancement—a field study in the Nicolet River: Canadian Journal of Civil Engineering, v. 34, p. 761–769, doi:10.1139/L06-083.

Cataño-Lopera, Y.A., and García, M.H., 2006, Burial of short cylinders induced by scour under combined waves and currents: Journal of Waterway, Port, Coastal, and Ocean Engineering, v. 132, p. 439–449, doi:10.1061/(ASCE)0733-950X(2006)132:6(439).

Cataño-Lopera, Y.A., Landry, B.J., and García, M.H., 2011, Scour and burial mechanics of conical frustums on a sandy bed under combined flow conditions: Ocean Engineering, v. 38, p. 1256–1268.

Chiew, Y.M., 1990, Mechanics of local scour around submarine pipelines: Journal of Hydraulic Engineering, v. 116, p. 515–529.

Coard, R., 1999, One bone, two bones, wet bones, dry bones—transport potentials under experimental conditions: Jour-

nal of Archaeological Science, v. 26, p. 1369–1375.

Coard, R., and Dennell, R.W., 1995, Taphonomy of some articulated skeletal remains—transport potential in an artificial environment: Journal of Archaeological Science, v. 22, p. 441–448.

Daniel, J., 2012, Heads and skulls as sediment sorters—an actualistic, CT-based study in taphonomy: Athens, Ohio University, Ph.D. dissertation, 350 p.

Dargahi, B., 1990, Controlling mechanism of local scouring: Journal of Hydraulic Engineering, v. 116, p. 1197–1214.

Dey, S., Raikar, R.V., and Roy, A., 2008, Scour at submerged cylindrical obstacles under steady flow: Journal of Hydraulic Engineering, v. 134, p. 105–109.

Dill, R.F., 1958, The burial and scouring of ground mines on a sand bottom: San Diego, California, Navy Electronics Lab Report No. NEL-861, 23 p.

Dixen, M., Sumer, B.M., and Fredsøe, J., 2013, Numerical and experimental investigation of flow and scour around a half-buried sphere: Coastal Engineering, v. 73, p. 84–105.

Dodson, P., 1973, The significance of small bones in paleoecological interpretation: University of Wyoming Contributions to Geology, v. 12, p. 15–19.

Dodson, P., 1973, The significance of small bones in paleoecological interpretation: University of Wyoming Contributions to Geology, v. 12, p. 15–19.

Dorrell, R.M., Peakall, J., Sumner, E.J., Parsons, D.R., Darby, S.E., Wynn, R.B., Özsoy, E., and Tezcan, D., 2016, Flow dynamics and mixing processes in hydraulic jump arrays—implications for channel-lobe transition zones: Marine Geology, v. 381, p. 181–193.

Dou, X.S., and Jones, J.S., 2000, A new sediment transport formula for local scour prediction, *in* Hotchkiss, R.H., and Glade M., editors, Building partnerships: American Society of Civil Engineers Proceedings of the 2000 Joint Conference on Water Resource Engineering and Water Resources Planning and Management, p. 1–8, https://doi.org/10.1061/40517(2000)410.

Droppo, I.G., D'Andrea, L., Krishnappan, B.G., Jaskot, C., Trapp, B., Basuvaraj, M., and Liss, S.N., 2015, Fine-sediment dynamics—towards an improved understanding of sediment erosion and transport: Journal of Soils and Sediments, v. 15, p. 467–479.

Ettema, R., Arndt, R., Roberts, P., and Wahl, T., 2000, Hydraulic modeling—concepts and practice: American Society of Civil Engineers Manuals and Reports on Engineering Practice, No. 97, 397 p.

Ettema, R., and Muste, M., 2004, Scale effects in flume experiments on flow around a spur dike in flatbed channel: Journal of Hydraulic Engineering, v. 130, p. 587–589, https://doi.org/10.1061/(ASCE)0733-9429(2004)130.

Euler, T., and Herget, J., 2011, Obstacle-Reynolds-number based analysis of local scour at submerged cylinders: Journal of Hydraulic Research, v. 49, p. 267–271.

Euler, T., and Herget, J., 2012, Controls on local scour and deposition induced by obstacles in fluvial environments: Catena, v. 91, p. 35–46.

Euler, T., Herget, J., Schlömer, O., and Benito, G., 2017, Hydro-morphological processes at submerged solitary boulder obstacles in streams: Catena, v. 157, p. 250–267.

Fernandez-Jalvo, Y., and Andrews, P., 2003, Experimental effects of water abrasion on bone fragments: Journal of Taphonomy, v. 1, p. 147–163.

Fernandez-Jalvo, Y., and Andrews, P., 2016, Atlas of taphonomic identifications—1001+ images of fossil and recent mammal bone modification: Dordrecht, Germany, Springer, 354 p., doi 10.1007/978-94-017-7432-1.

Fiorillo, A.R., 1994, Time resolution at Carnegie Quarry (Morrison Formation: Dinosaur National Monument, Utah)—implications for dinosaur paleoecology: Rocky Mountain Geology, v. 30, p. 149–156.

Foster, J.R., 2003, Paleoecological analysis of the vertebrate fauna of the Morrison Formation (Upper Jurassic), Rocky Mountain Region, USA: New Mexico Museum of Natural History and Science Bulletin 23, 95 p.

Franco, J.J., 1978, Guidelines for the design, adjustment and operation of models for the study of river sedimentation problems: U.S. Army Engineer Waterways Experiment Station Instruction Report H-78-1, 74 p.

Friedrichs, C.T., Rennie, S.E., and Brandt, A., 2016, Self-burial of objects on sandy beds by scour—a synthesis of observations, *in* Harris, J., Whitehouse, R., and Moxon, S., editors, Scour and erosion: Boca Raton, Florida, CRC Press, p. 179–189.

Frison, G.C., and Todd, L.C., 1986, The Colby Mammoth Site—taphonomy and archaeology of a Clovis Kill in northern Wyoming: Albuquerque, University of New Mexico Press, 238 p.

Gilmore, C.W., 1936, Osteology of *Apatosaurus*, with special reference to specimens in the Carnegie Museum: Memoirs of the Carnegie Museum, v. 11, p. 175–296.

Grayson, R.B., Moore, I.D., and McMahon, T.A., 1992, Physically based hydrologic modeling 2—is the concept realistic?: Water Resources Research, v. 26, p. 2659–2666.

Griffith, S.J., Thompson, C.E.L., Thompson, T.J.U., and Gowland, R.L., 2016, Experimental abrasion of water submerged bone—the influence of bombardment by different sediment classes on microabrasion rate: Journal of Archaeological Science Reports, v. 10, p. 15–29.

Haltigin, T.W., Biron, P.M., and Lapointe, M.F., 2007, Predicting equilibrium scour-hole geometry near angled stream deflectors using a three-dimensional numerical flow model: Journal of Hydraulic Engineering, v. 133, p. 983–988, doi:10.1061/(ASCE)0733-9429(2007)133:8(983).

Hanson, C.B., 1980, Fluvial taphonomic processes—models and experiments, *in* Behrensmeyer, A.K., and Hill, A.P., editors, Fossils in the making: Illinois, University of Chicago Press, p. 156–181.

Hoffmans, G.J., and Verheij, H.J., 1997, Scour manual: Boca Raton, Florida, CRC Press, 224 p.

Holland, W.J., 1915, Heads and tails—a few notes relating to the structure of the sauropod dinosaurs: Annals of Carnegie Museum, v. 9, p. 273–278.

Horritt, M.S., and Bates, P.D., 2002, Evaluation of 1D and 2D numerical models for predicting river flood inundation: Journal of Hydrology, v. 268, p. 87–99.

Inman, D.L., and Jenkins, S.A., 1996, A chronology of ground mine studies and scour modeling in the vicinity of La Jolla: Scripps Institution of Oceanography Reference Series No. 96–13, 26 p.

Inman, D.L., and Jenkins, S.A., 2005, Scour and burial of objects in shallow water, *in* Schwartz, M.L., editor, Encyclopedia of coastal science: Dordrecht, Germany, Springer, p. 825–830.

Istiarto, I., 2001, Flow around a cylinder in a scoured channel bed: École Polytechnique Fédérale De Lausanne, Ph.D. dissertation, 263 p.

Jenkins, S.A., Inman, D.L., Richardson, M.D., Wever, T.F., and Wasyl, J., 2007, Scour and burial mechanics of objects in the nearshore: Journal of Oceanic Engineering, v. 32, p. 78–90.

Johnson, R.G., 1957, Experiments on the burial of shells: Journal of Geology, v. 65, p. 527–535.

Kaufmann, C., Gutiérrez, M.A., Álvarez, M.C., González, M.E., and Massigoge, A., 2011, Fluvial dispersal potential of guanaco bones (*Lama guanicoe*) under controlled experimental conditions—the influence of age classes to the hydrodynamic behavior: Journal of Archaeological Science, v. 38, p. 334–344.

Kirkil, G., and Constantinescu, G., 2010, Flow and turbulence structure around an in-stream rectangular cylinder with scour hole: Water Resources Research, v. 46, w11549, 20 p., doi:10.1029/2010WR009336.

Kostaschuk, R.A., and Villard, P.V., 1999, Turbulent sand suspension over dunes, *in* Smith, N.D., and Rogers, J, editors, Fluvial sedimentology VI: International Association of Sedimentologists Special Publication 28, p. 3–14.

Lawton, R., 1976, Taphonomy and paleohydraulics—Morrison Formation, northeastern Utah: Santa Cruz, University of California, Senior Thesis, 67 p.

Lawton, R., 1977, Taphonomy of the dinosaur quarry, Dinosaur National Monument: University of Wyoming Contributions to Geology, v. 15, p. 119–126.

Lefeuvre, A.R., 1965, Sediment transport functions with special emphasis on localized scour: Atlanta, Georgia Institute of Technology, Ph.D. dissertation, 91 p.

Madsen, J.H., McIntosh, J.S., and Berman, D.S., 1995, Skull and atlas-axis complex of the Upper Jurassic sauropod *Camarasaurus* Cope (Reptilia: Saurischia): Bulletin of the Carnegie Museum of Natural History, v. 31, p. 1–115.

Maity, H., and Mazumder, B.S., 2014, Experimental investigation of the impacts of coherent flow structures upon turbulence properties in regions of crescentic scour: Earth Surface Processes and Landforms, v. 39, p. 995–1013.

Martinuzzi, R., and Tropea, C., 1993, The flow around surface-mounted, prismatic obstacles placed in a fully developed channel flow: Journal of Fluids Engineering, v. 115, p. 85–92.

Matgen, P., Schumann, G., Henry, J.B., Hoffmann, L., and Pfister, L., 2007, Integration of SAR-derived river inundation areas, high-precision topographic data and a river flow model toward near real-time flood management: International Journal of Applied Earth Observation and Geoinformation, v. 9, p. 247–263.

Mazumder, B.S., Maity, H., and Chadda, T., 2011, Turbulent flow field over fluvial obstacle marks generated in a laboratory flume: International Journal of Sediment Research, v. 26, p. 62–77.

Menzel, P., Rückborn, T., and Leder, A., 2013, Flow and scour around cylindrical objects in laboratory experiments: Proceedings of IEEE OCEANS 2013, Bergen, Norway, p. 1–8.

Millard, C., Hajek, E., and Edmonds, D.A., 2017, Evaluating controls on crevasse-splay size—implications for floodplain-basin filling: Journal of Sedimentary Research, v. 87, p. 722–739.

Minamoto, Y., 2013, Flowsquare 4.0: Theory and Computation, http://flowsquare.com.

Morris, R.S., 1997, The taphonomy and paleoecology of the late Miocene terrestrial vertebrate locality near northwest Iran—a framework for paleoenvironmental analysis of late Miocene Hominoidea: Los Angeles, University of Califor-

nia, Ph.D. dissertation, 467 p.

Nienhuis, J.H., Törnqvist, T.E., and Esposito, C.R., 2018, Crevasse splays versus avulsions—a recipe for land building with levee breaches: Geophysical Research Letters, v. 45, p. 4058–4067, doi.org/10.1029/2018GL077933.

Olsen, N.R., and Melaaen, M.C., 1993, Three-dimensional calculation of scour around cylinders: Journal of Hydraulic Engineering, v. 119, p. 1048–1054.

Orr, P.J., Adler, L.B., Beardmore, S.R., Furrer, H., McNamara, M.E., Peñalver-Mollá, E., and Redelstorff, R., 2016, "Stick 'n'peel"—explaining unusual patterns of disarticulation and loss of completeness in fossil vertebrates: Palaeogeography, Palaeoclimatology, Palaeoecology, v. 457, p. 380-388.

Pante, M.C., and Blumenschine, R.J., 2010, Fluvial transport of bovid long bones fragmented by the feeding activities of hominins and carnivores: Journal of Archaeological Science, v. 37, no. 4, p. 846–854.

Papanicolaou, A.N., Kramer, C.M., Tsakiris, A.G., Stoesser, T., Bomminayuni, S., and Chen, Z., 2012, Effects of a fully submerged boulder within a boulder array on the mean and turbulent flow fields—implications to bedload transport: Acta Geophysica, v. 60, p. 1502–1546.

Paterson D.M., 1994, Microbiological mediation of sediment structure and behaviour, *in* Stal, L.J., and Caumette P., editors, Microbial mats—structure, development, and environmental significance: NATO ASI Series G, Ecological Sciences, v. 35, p. 97–109.

Schumann, G., Bates, P.D., Horritt, M.S., Matgen, P., and Pappenberger, F., 2009, Progress in integration of remote sensing-derived flood extent and stage data and hydraulic models: Reviews of Geophysics, v. 47, RG4001, 20 p., doi:10.1029/2008RG000274.

Shipman, P., and Rose, J., 1988, Bone tools and experimental approach, *in* Olson, S., editor, Scanning electron microscopy in archaeology: British Archaeological Reports National Series, v. 452, p. 303–335.

Smith, H.D., and Foster, D.L., 2005, Modeling of flow around a cylinder over a scoured bed: Journal of Waterway, Port, Coastal, and Ocean Engineering, v. 131, p. 14–24.

Smith, H.D., and Foster, D.L., 2007, Three-dimensional flow around a bottom-mounted short cylinder: Journal of Hydraulic Engineering, v. 133, p. 534–544.

Southard, J.B., and Boguchwal, L.A., 1990, Bed configuration in steady unidirectional water flows—part 2, synthesis of flume data: Journal of Sedimentary Research, v. 60, p. 658–679.

Szupiany, R.N., Amsler, M.L., Parsons, D.R., Best, J.L., and Haydel, R., 2019. Comparisons of morphology and flow structure at two braid-bar confluences in a large river, *in* Dohmen-Janssen, C.M., and Hulscher, S.J.M.H., editors, River, coastal and estuarine morphodynamics: Boca Raton, Florida, CRC Press, p. 754–761.

Termini, D., 2011, Bed scouring downstream of hydraulic structures under steady flow conditions—experimental analysis of space and time scales and implications for mathematical modeling: Catena, v. 84, p. 125–135.

Thompson, C.E.L., Ball, S., Thompson, T.J.U., and Gowland, R., 2011, The abrasion of modern and archaeological bones by mobile sediments—the importance of transport modes: Journal of Archaeological Science, v. 38, p. 784–793.

Trapani, J., 1998, Hydrodynamic sorting of avian skeletal remains: Journal of Archaeological Science, v. 25, p. 477–487.

Tritico, H.M., and Hotchkiss, R.H., 2005, Unobstructed and obstructed turbulent flow in gravel bed rivers: Journal of Hydraulic Engineering, v. 131, p. 635–645, http://dx.doi.org/10.1061/(ASCE)0733-9429(2005)131:8(635).

Turner, C.E., and F. Peterson, 1992, Study of the Jurassic Morrison Formation at Dinosaur National Monument, Colorado and Utah [abs.]: Society for Sedimentary Geology (SEPM) Abstracts, p. 64.

Voorhies, M.R., 1969, Taphonomy and population dynamics of an early Pliocene vertebrate fauna, Knox County, Nebraska: University of Wyoming Contributions to Geology Special Paper No. 1, 69 p.

Weller, J.M., 1959, Compaction of sediments: American Association of Petroleum Geologists Bulletin, v. 43, p. 273–310.